

Riga Technical University
Faculty of Electronics and Telecommunications
Institute of Radioelectronics

Nikolajs Ponomarenko

Doctoral student of "Electronics" study program

**Study of Frequency and Microstructure
Dependencies of Magnetic Losses of Ferrite
Materials and Components**

Summary of the Doctoral Thesis

Scientific supervisor
Dr. habil. sc. ing., prof.
J. Jankovskis

Rīga 2014

UDK 621.318.13

Po 525 s

Ponomarenko N. Study of Frequency and Microstructure Dependencies of Magnetic Losses of Ferrite Materials and Components. Summary of Doctoral Thesis.– R.: RTU Press, 2014.– 55 p.

Published according to the decision of the Promotion Council RTU ETF „RTU P-08” of September 25, 2014, Nr. 23/1



This work has been supported by the ESF.

ISBN 978-9934-10-641-5

PROMOTION WORK
SUBMITTED FOR THE DEGREE OF A DOCTOR
OF ENGINEERING SCIENCES (ELECTRONICS) TO BE DEFENDED
AT RIGA TECHNICAL UNIVERSITY

The promotion work for a doctor's degree of engineering sciences (electronics) is to be defended publicly on 8th of January, 2015. At the faculty of Electronics and Telecommunications of Riga Technical University, 16/20 Azenes Str., in the lecture-room 215.

OFFICIAL REVIEWERS

Andris Ozols (professor, Dr. habil. phys., RTU, Institute of Technical Physics);

Juris Roberts Kalniņš (asoc. prof., Dr. habil. phys., Ventspils high school, Mathematics and Natural Sciences department);

Vera Skvorcova (senior researcher., Dr. phys., LU, Institute of Solid State Physics).

CONFIRMATION

I confirm that I have developed this promotion work for a doctor's degree of engineering sciences which has been submitted for reviewing at the Riga Technical University. The promotion work is not submitted in any other university for a scientific degree.

Nikolajs Ponomarenko (Signature)

Date:

The promotion work is written in the English language. It contains Introduction, 5 Chapters, Conclusion, and Bibliography, 5 Appendixes, 107 figures and illustrations, with the total number of 162 pages. The Bibliography has 194 titles.

TABLE OF CONTENTS

1	GENERAL DESCRIPTION OF THE WORK	6
1.1	INTRODUCTION	6
1.2	ACTUALITY OF RESEARCH OF POLYCRYSTALLINE FERRITES	7
1.3	THE PURPOSE OF THE WORK	9
1.4	PROVED THESIS	10
1.5	APPROBATION OF THE RESULTS	10
1.6	STRUCTURE OF THE THESIS	12
2	GENERALITIES OF FERRITE CHARACTERISTICS IN RELATION TO FREQUENCY	13
2.1	MAGNETIC LOSSES; LOSSES ACCORDING TO STEINMETZ EQUATION	13
2.2	COMPLEX PERMEABILITY	15
2.2.1	PROBLEMS OF PRESENTATIONS OF COMPLEX PERMEABILITY	17
2.2.2	ROLE OF MICROSTRUCTURE	17
2.2.2.1	Characteristics of microstructure	18
2.2.3	ROLE OF MICROSTRUCTURE ON FREQUENCY DEPENDENT CHARACTERISTICS OF PF	20
2.2.4	MODELING OF COMPLEX PERMEABILITY BY ACCOUNTING FOR THE EFFECTS OF MICROSTRUCTURE	21
2.2.5	FERRITES FOR SMPS	25
2.3	REVIEW OF FERRITE HF PROBLEMS	26
3	KRAMERS-KRONIG RELATIONS APPLICATION TO EXPERIMENTAL DATA	28
3.1	MAGNETIC SPECTRA QUALITY - ANALYSIS FROM KKR VIEWPOINT	28
3.2	DECOMPOSITION OF SPECTRA	30
4	STUDY OF MICROSTRUCTURE OF SAMPLES USED; MST ASPECTS FOR PF OF SMPS	31
4.1	STATISTICAL PARAMETERS OF FERRITE MICROSTRUCTURE	31
4.2	PREPARING OF SAMPLES WITH SIMILAR MICROSTRUCTURE	33
5	MEASUREMENTS OF FERRITE MAGNETIC AND DIELECTRIC PROPERTIES	35
5.1	EXPERIMENTAL RESULTS	35
5.2	COMPLEX PERMITTIVITY MEASUREMENTS	37
6	STUDY OF CORRELATION BETWEEN THE MODELING AND EXPERIMENTAL MS	38
6.1	INVESTIGATION OF SYMMETRICAL SPECTRA OF CIP	38
6.2	APPLICATION OF THE MODEL FOR PRESENTATION OF ASYMMETRICAL SPECTRA	39
6.2.1	PRESENTATION OF CIP SPECTRA OF NICKEL FERRITES	39
6.2.2	PRESENTATION OF CIP OF SAMPLES WITH IDENTICAL MICROSTRUCTURE	40
6.3	PRESENTATION OF CIP OF SAMPLES EXHIBITING DIMENSIONAL RESONANCE	42
6.4	COMPLEX INITIAL PERMEABILITY AS INTRINSIC AND EXTRINSIC PROPERTY	47
7	CONCLUSIONS AND FUTURE INVESTIGATIONS	49
7.1	CONCLUSIONS	49
7.2	FUTURE INVESTIGATIONS	51
	LIST OF LITERATURE	52

Main abbreviations

SMPS – switched mode power supply

PF – polycrystalline ferrite

InP – intrinsic property

ExP –extrinsic property

CIP – complex initial permeability

MST – microstructure

ACp – absorption component

DCp – dispersion component

DR – dimensional resonance

NSR – natural spin resonance

KKR – Kramers-Kronig relations

DW – domain wall

List of main physical values

f- frequency

$\dot{\mu}(f)$ – complex magnetic permeability

$\mu'(f)$ – complex permeability real part

$\mu''(f)$ – complex permeability imaginary part

$\tan\delta(f)$ – loss tangent

$f_u - \mu''(f)$ absorption maximum frequency

$\mu''_{max} - \mu''(f)$ absorption maximal value

D_a – average grain diameter

$f(D), f_{ln}(D)$ – probability density functions

$\mu'_{model}(f), \mu''_{model}(f)$ – model approximation real and imaginary components

f_a, f_b – the model specific frequency working points

σ_a, σ_b – the model specific dispersion working points

1 GENERAL DESCRIPTION OF THE WORK

1.1 Introduction

Nowadays technology and science is focusing on three global problems [53]: energy, environment and health. Magnetic materials can contribute in all of these cases (as improved performance of magnetic components, reduced electromagnetic interference (EMI) and better electromagnetic compatibility (EMC), or advanced medicine solutions). The soft magnetic materials (such as ferrites, nanocrystalline and amorphous materials, etc.), e. g., represent the *magnetics* "pillar" of power electronics (being one of the three traditional pillars of power electronics: power semiconductors; control; and magnetics [49]). Thus, the study of soft magnetic materials is significant not only in developing an up to date power electronics, which, in fact, is the main consumer of these materials.

The portable electronics units (especially – hand-held devices) tend to become lighter and smaller, even so maintaining high efficiency. While the signal processing parts of electronics (e. g., microprocessors) are following the Moore's Law, power supply electronics (based on the highest efficiency converters switched mode power supplies (SMPS)), is developing much more slowly: its power density is doubling only in every ten years [13]

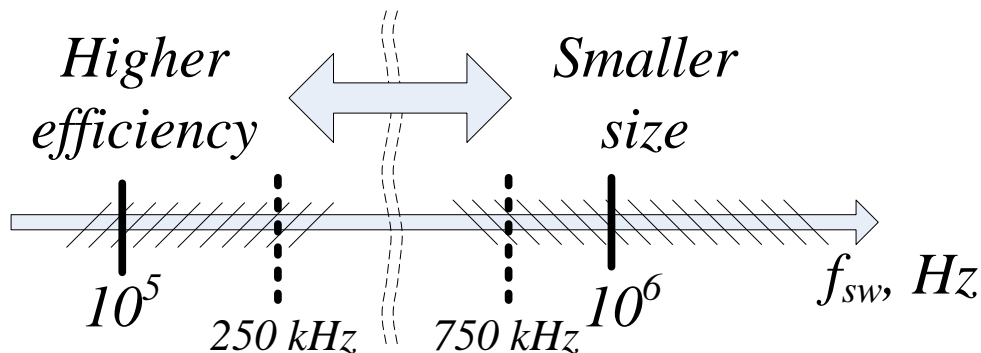


Figure 1.1 Power Integrations 500 W Hyper LCS family resonant converter efficiency and size dependence from frequency (data from [57])

(since 1970). Even this is obtained mainly through the use of higher switching frequencies, f_{sw} , which in their turn are growing by a factor approaching ten in recent decades [13]. The use of high f_{sw} affects nearly every performance characteristic of SMPS [54,55] and requires new attention to be placed on parasitic impedances, effects from printed circuit board (PCB) layout, potential sources of large output ripple switching spikes, and electromagnetic interference (EMI) – both conducted and radiated [43]. Therefore unjustifiably high f_{sw} often results in lower efficiency (as it is shown in Fig. 1.1 for Power Integrations 500 W Hyper

LCS family resonant converter [57]: it can be seen that there exists a gap between two possible choices - small size on operating at 750 kHz and maximum efficiency (up to 97 %) at 250 kHz). Other research [50] on the high frequency DC/DC converter TPS54160 gave similar results.

The solution provided in this connection is a design trade-off [41] either – the smaller size but the decrease of efficiency or highest efficiency possible with bigger size. Nevertheless – higher f_{SW} provides possibility for using smaller magnetic components in SMPS due to reduction of size of the core. The polycrystalline ferrites (PF) are the typical core materials for production of high efficiency components.

1.2 Actuality of research of polycrystalline ferrites

Nowadays, the PF remains the typical core materials used for the production of high efficiency components. For many high frequency (HF) applications of PF – for signal and switch mode power supply electronics as inductive components, for electromagnetic compatibility and wireless power supply as elements, components, and HF absorbing materials. The improvements of magnetics for SMPS mainly are related with that of polycrystalline ferrites (PF). They (especially MnZn and NiZn ferrites) are the common choice for inductive component cores applications within frequency range of several kilohertz to several megahertz. Besides, there are increasingly stringent requirements to dimensions, reliability, stability of inductive components in wide frequency range. This makes it to be more attentive to the choice of conventional ferrites (basing on deeper understanding of their nature) and dictates the trends for development of new ones. Often, the PF primary task is to concentrate and guide the magnetic flux. Potentially this and other functions are fulfilled, to a greater or lesser extent, by PF being found either as intrinsic or extrinsic substances. The term *intrinsic* in the context of this work is used for distinction between the characteristics of PF samples that directly depend on composition and structure of materials, and those as *extrinsic* ones affected by quantity and shape factors. It is quite clear that the definite characteristic of PF in accordance with the conditions may be as intrinsic property (InP) or extrinsic property (ExP). Still it remains to be mentioned that there is possible to distinguish two “degrees” of InP of PF samples in relation to their processing technology and resulting MST: *true “intrinsic”* in the case of microstructure without intragrain defects and *simply “intrinsic”* in the opposite case.

In many engineering applications of PF we are dealing with their ExP (in this study: the dimensional resonance, influence of width of nonmagnetic gap). Platform for study of ExP comes from that of intrinsic ones.

Turning back to the flux concentration, of most concern are the primary magnetic characteristics of the material: relative permeability (both static permeability, $\mu(0)$, and complex permeability (CP), $\dot{\mu}(f)$, specified within the frequency, f , range of interest) and the saturation parameters (the saturation flux density, B_S or the magnetization, M_S). The saturation parameters are universally available specifications not depending on the form of characterization of PF – as InP or ExP ones. Contrary to this CP $\dot{\mu}(f) = \mu'(f) - j\mu''(f)$ with $\mu'(f)$ as dispersion part, (component, DCp), and $\mu''(f)$ as the absorption part, (component, ACp), are more intricate characteristics which manufactures are specifying as a rule as InP for relatively small toroidal cores [61] and yet not always. And this in spite of reality that CP as InP and ExP typically differ widely, so their ability to concentrate the flux (typically under conditions of small magnetic losses) at the definite f . In the regards to losses CP is the key characteristic since HF losses of magnetic materials are directly related to CP, defining the value of magnetic loss tangent as: $\tan\delta(f) = \mu''(f)/\mu'(f)$. In addition, for obtaining high efficiency at higher power levels the magnetic cores should be designed with significantly larger dimensions than low-power cores (the available data, in general, represents the low power core specifications). But with larger dimensions of the core the new problem may arise that cannot be accounted using only specifications for low power ring cores. Such a problem is called the dimensional resonance (DR) in the core.

The subjects of research in this work are manganese zinc (MnZn) and nickel zinc (NiZn) ferrites, as these materials are most common for application in SMPS. To neglect the nonlinearity effects the samples in this study are investigated under the action of weak fields, i. e., in fact CP $\dot{\mu}(f)$ is viewed as complex initial permeability (CIP). The results gained for weak fields are assumed as platform for higher fields and non-sinusoidal excitations [63, 64].

From the many characteristics of PF the complex initial permeability frequency dependence (also called the magnetic spectra, MS), and it's interrelation with PF microstructure (MST) is mainly studied in this work. So, here CIP mostly appears as InP, but there are also provided experimental data relating to the dimensional resonance (as ExP).

Despite the fact, that CIP as an important PF characteristics is studied for decades, there still has not been developed a physically reasonable mathematical model which is in correspondence with experiments; existing approximations are formal and with significant

drawbacks – they do not include the influence of MST of PF. An important role in this work has the experimental CIP spectra: they are measured within this study, and, also there are used CIP spectra from other measured data (some of them were refused because they did not correlate with Kramers-Kronig relationship (KKR) [65]; also there often are problems with MST characteristics).

Table 1.1 Magnetic and geometrical parameters of studied ferrite samples

Group	№	Dimensions, mm	$\mu(0)$	<i>The making of samples</i>
	A1	R12 × 8 × 6	2000	
NiZn, 4S60	A2	R20 × 10 × 6	2000	<i>Cut from ferrite tile</i>
	A3	R31.5 × 20.5 × 6	2000	
	A4	R40 × 23.5 × 6	2000	
MnZn, 6000HM1	B1	R10 × 4.3 × 10	6000	<i>Cut from ferrite tile</i>
	B2	R20 × 9.1 × 10	6000	
	B3	R25 × 12 × 10	6000	
	B4	R30 × 14.3 × 10	6000	
	B5	R33 × 10 × 10	6000	
MnZn, TDK T37	C1	R12.5 × 7.5 × 5	6500	<i>Commercial products</i>
	C2	R20 × 10 × 7	6500	
	C3	R40 × 24 × 16	6000	

The analytical modeling of CIP based on grain size distribution effects (developed by the supervisor) is described and experimentally proved. Experimental measurement frequency range was taken so to obtain most of large amplitude broadband absorption region of CP.

1.3 The purpose of the work

Objectives arise from the research: basing on experimentally obtained CIP and MST data for the PF groups (MnZn and NiZn), to prove (or to reject) the developed (hypothetical) CIP analytical model based on polycrystal grain size distribution effects.

The purpose of this work lies in:

- investigate the problems of presentation of complex initial permeability including the frequencies of large amplitude broadband dispersion (domain wall one);

- study of PF microstructure with the aim to form the basis for more deep understanding and modeling capabilities of complex permeability;
- study of the complex initial permeability in accordance with the microstructure (which is characterized by the mean grain size and size dispersion).

In this work there are analyzed problems, based on experimental study of complex magnetic permeability, verification of obtained spectra quality and study of large cores (in relation to dimensional resonance effect). The quality of obtained magnetic spectra was verified by MATLAB program, based on Kramers-Kronig relations.

1.4 Proved thesis

In this work there are offered and proved the following theses:

- that losses, which are connected with main absorption region of magnetic permeability as frequency characteristic of ferrite material, can be presented analytically by the modeling based on polycrystal grain size distribution effects;
- that CIP as intrinsic characteristic of polycrystalline NiZn and MnZn (small sample) ferrites is possible to present by modeling based on microstructure effects;
- that CIP as extrinsic characteristic of sufficiently large MnZn ferrite samples exhibit dimensional resonance which (along with already known factors) depends on number of turns of measuring winding, but variations of characteristics of spectra are not following Snoek's Law type relations;
- that Kramers-Kronig relations are powerful tool both for their use for verification of quality of magnetic spectra, and for decomposition, extrapolation and physically reasonable interpretation of compound magnetic spectra as a whole.

1.5 Approbation of the results

The main results of the work were presented on following conferences:

- The 8th international scientific and practical conference, Rezekne, Latvia, June 20–22, 2011;
- The 7th International conference on functional materials and nanotechnologies (FM&NT), Riga, Latvia, April 17–20, 2012;
- The 2nd international conference on materials and applications for sensors and transducers (ICMAST), Budapest, Hungary May 24–28, 2012;
- The 17th International conference “Electronics’ 13”, Kaunas, Lithuania, June 17–19, 2013;

- The 8th International conference on functional materials and nanotechnologies (FM&NT), Tartu, Estonia, April 21–24, 2013;
- The 21st International conference on soft magnetic materials (SMM-21), Budapest, Hungary, 1–4 September, 2013.

And there are published six publications:

1. J. Jankovskis, N. Ponomarenko, P. Narica. An Investigation on High Frequency Permeability of Polycrystalline Ferrites. *Proceedings of the 8th International Scientific and Practical Conference, Latvia, Rezekne, 20–22 June, 2011 – pp. 194–201.*
2. J. Jankovskis, N. Ponomarenko, N. Mironova-Ulmane, D. Jakovlevs. Dimensional effects of sample geometry and microstructure of MnZn and NiZn ferrites. *2012 IOP Conf. Ser.: Mater. Sci. Eng.* **38** 012018 – pp. 1–4.
3. J. Jankovskis, N. Ponomarenko, D. Stepins. Frequency Dependence of Complex Permeability of Polycrystalline Ferrites Based on the Realities of Microstructure. *Key Engineering Materials*, 543, 2013, – pp. 507–510.
4. J. Jankovskis, D. Stepins, N. Ponomarenko. Effects of Spread Spectrum on Output Filter of Buck Converter. *Electronics and Electrical Engineering*, 2013, Vol. 19, No. 5, pp. 45–48. e-ISSN 2029-5731. ISSN 1392-1215.
5. J. Jankovskis, N. Ponomarenko, N. Mironova-Ulmane, D. Jakovlevs. The study of correlation between microstructure of ferrites and their complex permeability spectra. *2013 IOP Conf. Ser.: Mater. Sci. Eng.* **49** 012045 – pp 1–4.
6. J. Jankovskis, N. Ponomarenko. Complex permeability of ferrites as intrinsic and extrinsic properties. *J. Chem. Chem. Eng.* 8 (2014) pp. 85–91

The first publication is indexed in Rezekne Higher Educational Institution database (<http://zdb.ru.lv>) . The publications 2, 3, 4 and 5 are indexed in SCOPUS and IOP databases. The 6th publication is indexed in databases of Cambridge Science Abstracts (CSA); Ulrich's Periodicals Directory, Database of EBSCO, USA; Chinese Scientific Journals Database, VIP Corporation, Chongqing, China; Chinese Database of CEPS, American Federal Computer Library center (OCLC), USA; Chemical Abstracts Service (CAS); Google Scholar; Proquest, USA; CCRIS; ChemID Subset; DIRLINE; Gene-Tox, HSDB; TOXLINE/Subset; Publicon Science.

1.6 Structure of the thesis

The first chapter of the thesis provides an overview of the problems associated with high frequency applications of ferrites.

The brief review of the ferrite losses in relation to frequency (static hysteresis loss, classical eddy-current loss and anomalous loss) is drawn in second chapter. The Steinmetz empirical approach and complex permeability analysis of the CIP are described. The modeling based on the grain distribution effects is presented in this chapter. An overview of the problems associated with the use of PF in SMPS is presented at the end of the chapter.

The analysis of experimental magnetic spectra quality by the means of Kramers-Kronig relations is provided in chapter 3. Also, with help of KKR there is shown magnetic spectra decomposition possibility.

The fourth chapter provides actual examples of the study of ferrite microstructure, and related problems, in a review of the literature. Experimental results, based on the Saltikov's method, are presented for each ferrite group studied.

The fifth chapter presents different CIP measurement techniques and the experimental CIP measurements results. The quality of obtained experimental CIP spectra was tested with KKR. In the study of CIP the DR phenomena and its dependence from the number of measuring winding turns was found.

Chapter 6 uses background provided by the previous chapters (i. e. the microstructure analysis and measured CIP data) to experimentally test the analytical model. The analysis of samples exhibiting the dimensional resonance is presented in this chapter too.

Conclusions and possible future investigations are drawn in Chapter 7.

2 GENERALITIES OF FERRITE CHARACTERISTICS IN RELATION TO FREQUENCY

2.1 Magnetic losses; losses according to Steinmetz equation

The frequency dependence of the characteristics of magnetic components must be taken into account in the design of SMPS (as it affects the performance of the whole device) and in designing the filter components (as it affects the effectiveness of dealing with unwanted signals). There are two sources of the losses in magnetic components: losses in windings and in the core material [15]. The winding losses are fairly well described [40, 68], but the study of core losses (CL) still remains current. Therefore, in modeling of SMPS it is essential to correctly account for CL in order to raise efficiency of the SMPS [14]. The total core power loss (per unit volume) usually is separated [5, 51, 66] into components (typically for metallic materials, but even sometimes for PF as well):

- quasi-static hysteresis loss: $P_h = k_h f B_m^n$ (Steinmetz form); (2.1)

- classical eddy-current loss $P_e = \frac{\pi^2 d^2}{6 \rho} f^2 B_m^2$; (2.2)

- anomalous (often termed as residual for ferrites and excess for metallic materials) loss $P_a = \text{const}(f B_m)^{3/2}$ for iron-based materials [4] and no analytic representation for ferrites.

Graphical display of components of total loss usually [5, 51] is done with help of loss energy $W_i = P_i/f$, where P_i stands for specific loss (Fig. 2.1). Dealing with the loss energies (W_i) instead of power losses removes one power of frequency dependence of material power loss and thus the separation of losses becomes more descriptive (constant W_h , linearly growing W_e and the rest as W_a). Generally adding up of W_h and W_e gives the value that is less

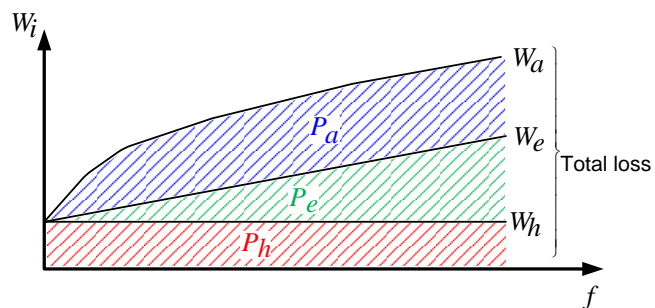


Figure 2.1. PF loss separation, adapted from [5].

than experimentally observed (total) value $W_{tot}(f) \equiv W_{exp}(f)$. To eliminate this discrepancy there is introduced anomalous loss $W_a = W_{exp}(f) - [W_h + W_e(f)]$.

The anomalous loss is still not adequately defined both physically and mathematically. In [14] are listed several possible reasons for this phenomenon in metallic ferromagnets: occurrence of domain walls; lack of flux penetration; non-sinusoidal flux density; interaction

between grains, grain size, grain orientation, and specimen thickness. Most of these reasons are obviously related to the high level of excitation fields (in metallic materials). Nevertheless, PF in SMPS at frequencies above 500 kHz are normally used (because of rapid growth of loss with frequency) at low level fields (near 50 mT, [6]), i. e., at fields much lower than the saturation field (typically ~ 500 mT). To this must be added the opinion [75] that P_e and P_a are difficult to obtain separately. In this situation it is possible to assume that a considerable contribution to anomalous loss comes from the dynamics of DW in grains of PF which can be represented by the frequency dependence of complex permeability (in [44] this contribution is termed as relaxation/resonance loss). Thus the study of complex permeability may provide more clearer understanding of excess loss as well.

It is seen from Fig. 2.1 that total loss is formed from three components: hysteresis loss; eddy loss; and anomalous (excess, residual) loss. From Eqs. (2.1) and (2.2) it follows that as $B_m \rightarrow 0$ the remaining part of the loss is the residual loss. The residual (anomalous) loss tangent is defined as $\tan\delta_a$ [66] (without a known analytical representation).

The total loss factor [66] can be written as (using loss tangent specific expressions):

$$\frac{\tan\delta_m}{\mu} = \frac{4k_h B_m}{3\pi\mu_0\mu^2} + \frac{\pi\mu_0\mu d^2 f}{\rho\beta} + \frac{\tan\delta_r}{\mu} \quad (2.3)$$

where k_h – hysteresis coefficient, B_m is the peak value of magnetic flux density, μ_0 – vacuum permeability, μ – material permeability, d – diameter (for toroidal samples), f is the sinusoidal operation frequency, ρ – resistivity, β – constant [66]. Thus the magnetic loss sources are with different dependence on f and B_m , the knowledge of which are essential for designers of power supplies to predict the losses when implementing a new power supply. In the following subchapters there will be provided total loss analysis based on Steinmetz approach (in fact, for a particular material, with determined empirical constants, and limited frequency and induction areas) and the complex permeability based approach (with significantly more universal frequency relation, but of limited induction).

In view of the fact that the components of magnetic loss of materials are not well separated and both hysteresis and eddy current loss are frequency and flux density dependent, the total loss is often in practice (not only that of magnetic core manufacturers', but scientific investigators' as well) still represented formally by the empirical Steinmetz equation (SE) (also known as the Power Law equation [14]):

$$P_{core} = k f^\alpha B_m^\beta \quad (2.4)$$

where P_{core} is the magnetic core average loss power dissipation per unit volume; k, α, β are the material dependent empirical coefficients determined by best fitting of the measured data

(for ferrites α is between 1.1...1.9, β is in range 1.6...3 [9]). In its original form (2.4) is usable only for sinusoidal signals. In addition it can work only in a limited range of frequencies and flux density excitations [72].

More clear physical content of Steinmetz type relations may be derived from the magnetic core series equivalent circuit with an ideal winding:

$$P = (\tan\delta/\mu_0\mu_r)\pi f B_m^2 \quad (2.5)$$

Considering the relation in more general case when the parameters incorporated may have dependence on f and B_m , i. e., $\tan\delta \equiv \tan\delta(f, B_m)$; $\mu_r \equiv \mu_r(f, B_m)$, and knowing their implicit functions the closed-form of Steinmetz relation can be derived (it is particularly remarkable that relation similar with Eq. (2.5) was derived by Landau-Lifschitz [74] as well using electromagnetic field approach).

2.2 Complex permeability

The magnetic permeability and magnetic losses are significant factors in designing of magnetic components [8]. The total loss (schematically presented in Fig. 2.1) consists of the eddy-current, hysteresis and anomalous losses. The eddy current losses becomes higher with increased frequency and hysteresis loss increases with increasing amplitude of the AC field [8]. As it was previously described, the anomalous loss is not mathematically defined and still cannot be fully described with empirical equations. According to observations (and curves shown on Fig. 2.1 as well) the anomalous loss is frequency dependent, thus it can be described (at least partly) with the frequency dependent characteristic of material, e. g., complex magnetic permeability $\dot{\mu}(f)$. In [36] – it was shown, that in specific case – under the action of low frequency and small fields the anomalous loss can be described with the complex initial permeability.

In general, if the alternating magnetic field $H = H_m e^{j\omega t}$ is applied to ferrite material – then associated flux density B is usually delayed by the phase angle δ due to losses ($B = B_m e^{j\omega t - j\delta}$). Magnetic permeability then is a complex characteristic:

$$\dot{\mu} = \frac{\dot{B}}{H} = \frac{B_m e^{j\omega t - j\delta}}{H_m e^{j\omega t}} = \frac{B_m}{H_m} e^{-j\delta} = \frac{B_m}{H_m} \cos\delta - j \frac{B_m}{H_m} \sin\delta = \mu' - j\mu'' \quad (2.6)$$

In equation (2.6) μ' is the real part; it characterizes the B component that is in phase with H . Imaginary part μ'' characterizes the B component that is delayed by $\pi/2$ phase-angle from H . Then from the (2.6) the loss factor tangent can be characterized as: $\tan\delta = \mu''/\mu'$.

Previously in the seventies and eighties (mainly by investigations inspired by the basic works of A. Globus and his collaborators, e. g., [21]) it was stated that CIP definitely depended on microstructure characteristics (more markedly on average grain size D_a) and that the dominating magnetization mechanism is domain wall (DW) displacement (nevertheless, at times however there appear groundless claims that the dominating magnetization process is the spin rotation [70]). In fact, if magnetic spectra (MS) data are taken over a really broad frequency range there can be found in the most general case, three dispersion regions [26] (see Fig. 2.2, experimental data are taken from [26]):

- a) in kHz range – relaxation type diffusion after effect (DIF), not always presented;
- b) in the decades near 1 MHz – the large amplitude dispersion attributed to DW processes;
- c) at microwaves (near several 100 MHz) – the small amplitude dispersion related to the natural spin resonance (NSR).

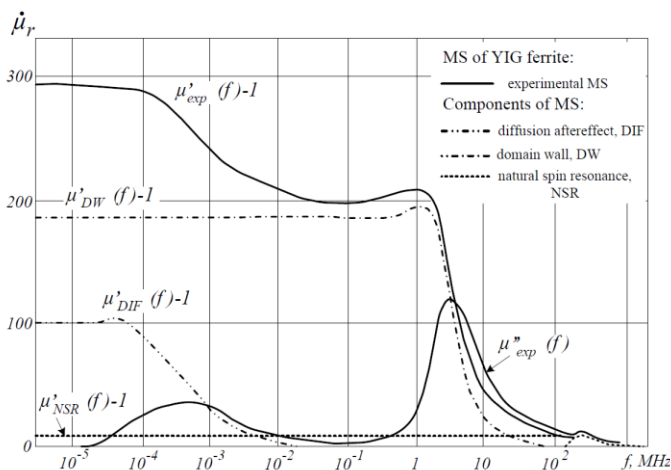


Figure 2.2 CP spectra decomposition [36]: the experimental ACp $\mu''(f)$ firstly is broken into three absorption components, from which were calculated corresponding DCp components: $\mu'_{DW}(f)$, $\mu'_{DIF}(f)$, $\mu'_{NSR}(f)$ by KK relations.

The DW displacement results in a larger DCp and ACp components than NSR, and therefore accounts for the high permeability of ferrites [8]. The NSR becomes of significance for higher frequencies (> 100 MHz), where it is dominant [8]. The contribution of each process into the whole CIP spectra becomes clearer, e. g, after decomposition of ACp $\mu''_{exp}(f)$ into the three mentioned components [36] (Fig. 2.2) and calculation of DCp $\mu'(f)$ by the use of Kramers-Kronig relations (3.1; 3.2).

For aforementioned it is more likely, that within the radiofrequency range (at room temperatures) for spinel and garnet type PF (most often used in practice) typically are dominating DW processes. Similarly as in Fig. 2.2 the contribution from NSR process in the total permeability $\mu(f)$ of a sample is often small and frequency independent up to very high frequencies; this is why the modeling of CIP is restricted over the region of large amplitude

dispersion as DW processes. The modeling of complex permeability spectra under the action of low fields in fact deals with the anomalous loss [36].

2.2.1 Problems of presentations of complex permeability

The modeling of typical complex permeability spectra presents difficulties in the correct representation of components (Fig. 2.3): DCp often exhibit resonance attributes (positive ups and negative downs, Fig. 2.3), ACp is asymmetrical (along log f scale axis) and broadband (often extending over several decades of f). Researchers for a long time now have measured a great quantity of different

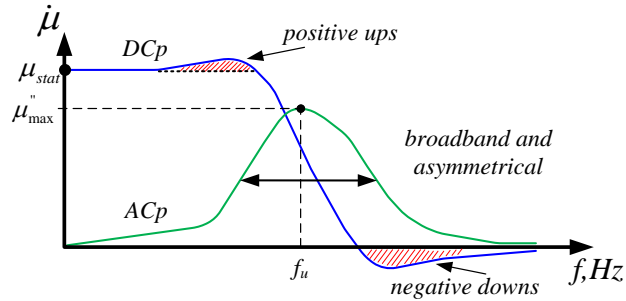


Figure 2.3 Typical complex permeability spectra

complex permeability spectra; clearly, there are several approaches to their approximations.

The simplest one is simple relaxation (with only one relaxation time τ), in form of complex magnetic permeability [36]:

$$\mu'(f) = \frac{\mu_{stat}}{1+(\tau f)^2}; \mu'' = \frac{\mu_{stat}\tau f}{1+(\tau f)^2} \quad (2.7)$$

where μ_{stat} is static value of CIP, f is the frequency, and τ – is the relaxation time. Even with the fact that this approximation of MS is pronouncedly broad, a closer look at typical DCp (Fig. 2.3) reveals that there may be clear evidence of resonance attributes as well, which it is not possible to represent by relaxation relations.

If MS is approximated by the use of simple harmonic oscillator relations:

$$\mu'(f) = \frac{\mu_{stat}f_0^2(f_0^2-f^2)}{(f_0^2-f^2)^2+4\xi^2f_0^2f^2}; \mu''(f) = \frac{2\mu_{stat}\xi f f_0^3}{(f_0^2-f^2)^2+4\xi^2f_0^2f^2}, \quad (2.8)$$

with ξ as the normalized damping *constant* (in the case of $\xi < 0.5$ the resonance features can be reproduced [36], but the ACp then becomes too narrowbanded).

Sometimes, in publications, the combination of relaxation and resonance approaches is used. The main limitations of this approach are its formality and clear ignorance of the effects of microstructure of PF on its CIP [26].

2.2.2 Role of microstructure

Undoubtedly several of important characteristics of PF are its microstructure (MST) sensitive (e. g., complex initial permeability $\mu(f)$ with its attributes: static initial permeability $\mu(0)$; typical representatives of ACp: μ''_{max} and f_u). To study the influence of MST on such

characteristics (e. g., CIP) there is need for proper MST characterization to perform the quantitative account of it.

2.2.2.1 Characteristics of microstructure

First of all, MST of PF (Fig. 2.4 a) is characterized by the law of its grain size D distribution. According to [42] MST obtained in the process of normal grains growth (NGG) almost without exceptions can be represented by log-normal distribution (independently of the material of sample, specific details of preparation conditions, grain sizes and density):

$$f_{\ln}(D) = \left(\frac{1}{D\sigma_{\ln}\sqrt{2\pi}}\right)e^{-\frac{(\ln D - \ln D_{med})^2}{2\sigma_{\ln}^2}}; \quad f(D) = \left(\frac{\log e}{D\sigma_D\sqrt{2\pi}}\right)e^{-\frac{(\log D - \log D_{med})^2}{2\sigma_D^2}} \quad (2.9)$$

where $f_{\ln}(D)$ and $f(D)$ are the probability density functions, D_{med} is the median of $\ln D$ or $\log D$ distribution, but the standard deviations σ_{\ln} and σ_D correspondingly are interrelated: $\sigma_{\ln} = \ln 10 \sigma_D = 2.3\sigma_D$. According to [42] MST obtain in the process of NGG for ferrites gives $\sigma_{\ln} = 0.45 \dots 0.55$ (or $\sigma_D = 0.2 \dots 0.24$).

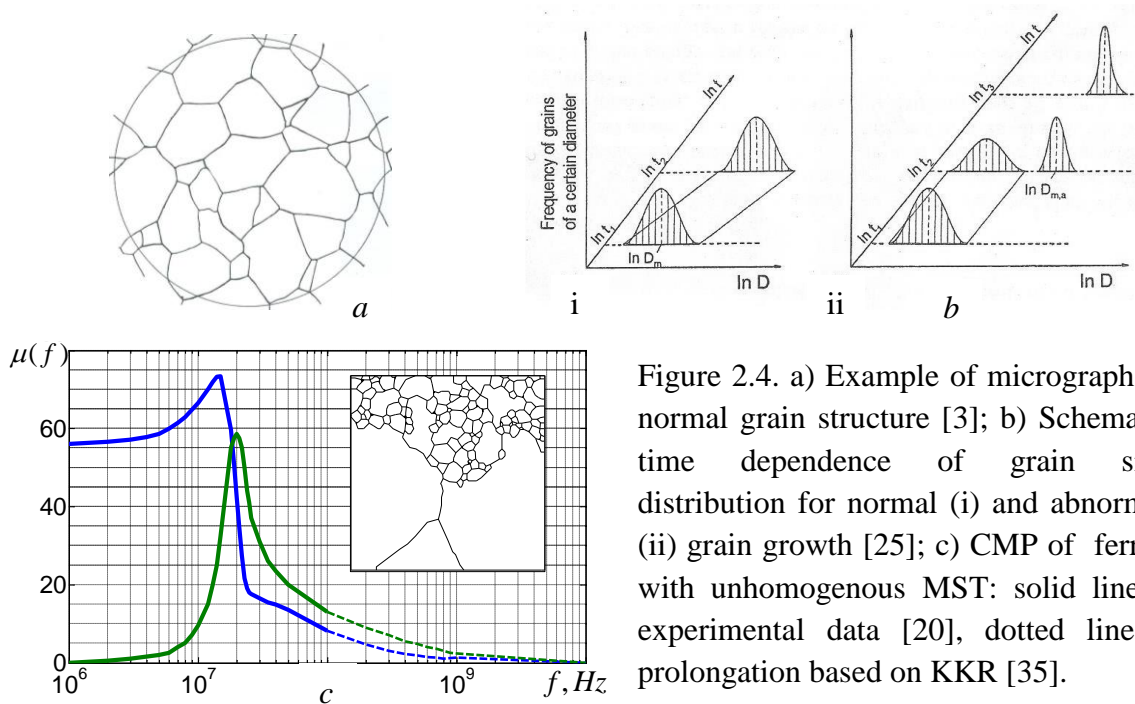


Figure 2.4. a) Example of micrograph of normal grain structure [3]; b) Schematic time dependence of grain size distribution for normal (i) and abnormal (ii) grain growth [25]; c) CMP of ferrite with unhomogenous MST: solid line – experimental data [20], dotted line – prolongation based on KKR [35].

The next important characteristic of MST is its average (mean) grain size $D_a = D_{med}e^{0.5\sigma_D^2 \ln^2 10}$. Contrary to the law of distribution, D_a is preparation conditions (mostly of sintering temperature and time) dependent. Within the normal grain growth the average grain size increases continuously with the increase of sintering time. Contrary to this abnormal grain growth leads to rapid growth of a few grains, while the other grains grow slowly or not at all [25], and the bimodal distribution appears (Fig. 2.4, b; the one distribution represents

the slowly-growing small-grained matrix, the other – rapidly growing grains). The distribution of slowly-growing grains becomes smaller and finally disappear (without changes of average grain size), oppositely – the distribution of abnormal grains (involving considerable amount of intragrain porosity) – changes within annealing time until abnormal grain growth ends (Fig. 2.4, b) [25]. This abnormality of grain growth forms unhomogeneous MST that correspondingly changes the typical form of CIP spectrum (Fig. 2.4, c).

The fundamental importance of D_a became widely evident from original investigations within the last decades of twenty century of A. Globus, M. Guyot and their collaborators on PF of special technology (from many publications highlighting only two the most comprehensive: [21], [26]). This technology includes: the composition of PF from oxides of high purity; the use of uncontaminating milling of oxides; the sintering at relatively low temperatures;

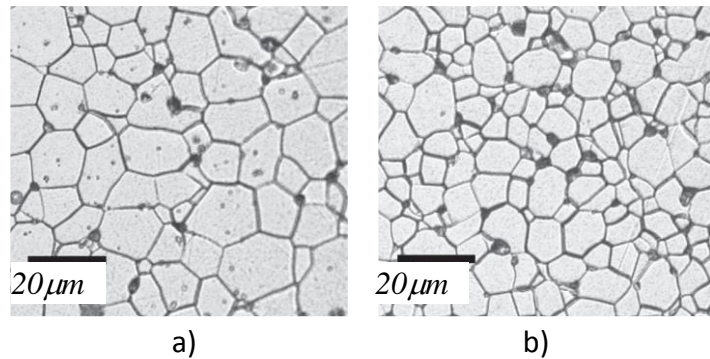


Fig. 2.5. Microstructures of (a) MB3 and (b) MBF4 ferrite materials [24] with the average grain sizes of $9 \mu\text{m}$ and $6 \mu\text{m}$, respectively.

a. o. [21]. All this results in PF samples of top quality: with homogeneous (i. e., log-normal) MST, porosity practically only as intergranular (intergrain) one, and grains without intragranular (intragrain) porosity. Such a porosity plays a minor role on the magnetization process attributes of whole PF sample if it results from magnetization processes of independent grains – several total characteristics of PF sample becomes MST dependent. Only the investigations on PF of this special technology, samples of top quality allow to reveal the true intrinsic nature of PF (in several previous publications these samples are referred to as: RSG – reference sample group, IQG – intrinsic quality group, or simply group one, PF1).

Real quality of MST (e. g., perfection of grains) to a large measure depends on the current value of D in the sample since it is resulting from actual processing technology of PF and laws of MST formation (e. g., in [12] it is stated that the pore-to-pore distance of intrapped pores does not change significantly when the MST changes from inter- to intragranular porosity).

Consequently the microstructure presented on Fig. 2.5 shows that there are defects mainly within coarser grain on PF (with $D \approx 9 \mu\text{m}$, Fig. 2.5, a), but intragrain defects almost

disappear within finer grained sample (with $D \approx 6 \mu m$ Fig. 2.5, b). Principles of inverse segregation and carried out direct experiments allows to conclude more generally that smaller grains within PF samples ($D < 3 \dots 5 \mu m$ [52]) are rather perfect – with the negligible amount of enclosed defects (e. g., porosity). For the coarser grains the picture decisively depends on technology.

2.2.3 Role of microstructure on frequency dependent characteristics of PF

Practice shows that several characteristics of CIP (more notably, $\mu(0) \equiv \mu_{stat}$ and f_u Fig. 2.3.) are interrelated. The knowledge of specific relationships of these interrelations are important for modeling of CIP. The process of setting up the relationships is not straightforward: it is not possible to base on definite theory (since there is no appropriate one) and so there is need to examine the empirical statistics of characteristics from great number of experimental CIP from publications all over the world. For this purpose in [29, 31] were analyzed large amount of ferrite sample data (over 100, produced by different technologies).

From the performed analysis of data there can be uncovered some regular trends which are possible to present by two pairs of empirical relations, individually revealing the true intrinsic and intrinsic properties of PF correspondingly:

$$\left. \begin{aligned} (\mu_s - 1)f_u D_a &= 12\pi M_s \\ \mu''_{max} f_u D_a &= (6 \dots 8)\pi M_s \end{aligned} \right\} \quad \left. \begin{aligned} (\mu_s - 1)f_u &= 4\pi M_s \\ \mu''_{max} f_u &= 2\pi M_s \end{aligned} \right\} \quad (2.10)$$

It can be seen that the first pair translates to second one at $D_a = (3 \dots 4) \mu m$. To interpret these results it is appropriate to introduce the effective grain size D_{eff} [29] reflecting the pinning situation of DWs in the grains of PF samples.

In the case of DW pinned only at grain boundaries (as in Globus' model [21]; Fig. 2.7: a, b) that is expected in the true intrinsic samples, $D_{eff} \approx D_a$ and as a

such is shown as linear relationship for all D_a (Fig. 2.6, line No. 1), meeting D_a axis in the range of very small, monodomain grains, D_{a0} . In this case all magnetization processes connected with DWs depend on D_a : influence of microstructure as *per se* appears in full measure.

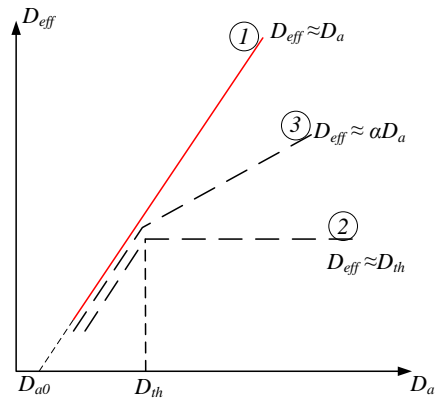


Figure 2.6. Conception of effective grain size D_{eff} : possible relationships between D_{eff} and D based on domain-wall processes in grains [29, Fig. 6]

Contrary to this in the case of (simply) intrinsic samples (of conventional ceramic technology) there are appearing the intragrain defects in the grains, pinning DWs (Fig. 2.7, c). However, from a number of experimental data it is possible to state, that small grains (less than $3...5 \mu m$ [52]) are without intragranular defects, so there is appearing some threshold size of grains, D_{th} .

Above provided analysis of the data for usual technology, non-specialized PF obviously gives (Eqs. 2.10) $D_{th} = (3...4)\mu m$, but in the case of specialized ones the results may be different (as in the example of power MnZn-ferrites optimized for higher frequencies $D_{th} < 6 \mu m$, [24]; but for higher initial permeability $D_{th} < 15 \mu m$ [12]). Since the pore-to-pore distance may be practically independent of D [12], then D_{eff} for $D > D_{th}$ may become $D_{eff} \approx D_{th} = const$ and

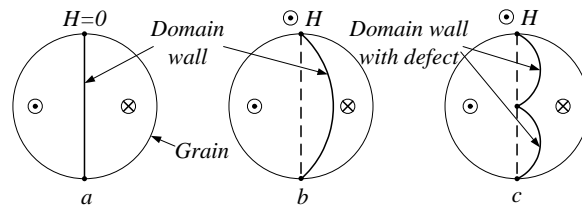


Figure 2.7. Schematic presentation of DW within a grain: a, b – Globus' model in a spherical grain without and with applied field; c – with applied field and pinning defect in the center of grain.

take a general view of dependence of No. 2 (Fig. 2.6); obviously, a compromise between No. 1 and No. 2 (dependence No. 3, Fig. 2.6) may take a place as well. Clearly, in the last two cases the influence of MST on parameters of PF is obscured, the correct results can be obtained only on intrinsic group samples. In this case it is possible to relate the magnetization process directly to material MST and to apply quantitatively to the general concept that experimentally observed characteristics of the sample in fact are integral ones appearing as such in the process of natural averaging their inner parameters over the ranges set up, e. g., by the grain size distribution.

2.2.4 Modeling of complex permeability by accounting for the effects of microstructure

Typically, the overall appearance of most CIP spectra are similar: they look like the combination both of relaxation attributes (dispersion and absorption within a broad range of frequency) and resonance attributes (positive ups and negative downs on $\mu'(f)$ – the dispersion curves). It was shown in [23] that in such a case the most appropriate approximation comes from taking account of inhomogeneous broadening of absorption caused in fact by the distribution of grain sizes (Fig. 2.9, a).

This concept translated to MS for ferrites from IQG, assumes that every polycrystal grain of the sample can be considered as a low loss oscillator (the DW in a current grain having $\mu_{stat} \propto D$ and resonating at $f_{osc} \propto 1/D^2$ with D standing for the current grain size). As a consequence the whole curve of ACp $\mu''(f)$ can be made up from absorption curves of these tiny oscillators (having the absorption line $\mu''_{osc}(f)$) with continuously distributed f_{osc} (for clarity in Fig. 2.8, a) the principle is shown as if ACp $\mu''(f)$ would be made up only by a group of a few oscillators). Accepting further that the grain size distribution probability density function is log-normal:

$$f(D) = (1/D\sigma_{\ln D}\sqrt{2\pi})\exp[-(\ln D - \ln D_{med})^2/2\sigma_{\ln D}^2] \quad (2.11)$$

where D_{med} is the median, and $\sigma_{\ln D}$ is the standard deviation of $\ln D$. The value of $\sigma_{\ln D}$ for PF with MST formed in the process of normal grain growth (i. e., with normal MST) tends to values [42]:

$$\sigma_{\ln D} \approx 0.5 \quad \text{or} \quad \sigma_{\log} \equiv \sigma_D = \sigma_{\ln D}/\ln 10 \approx 0.22 \quad (2.11^*)$$

– the latter value emerges in the case when (2.11) is presented on a decimal logarithmic scale that is more appropriate for CIP analysis in the frequency f -domain.

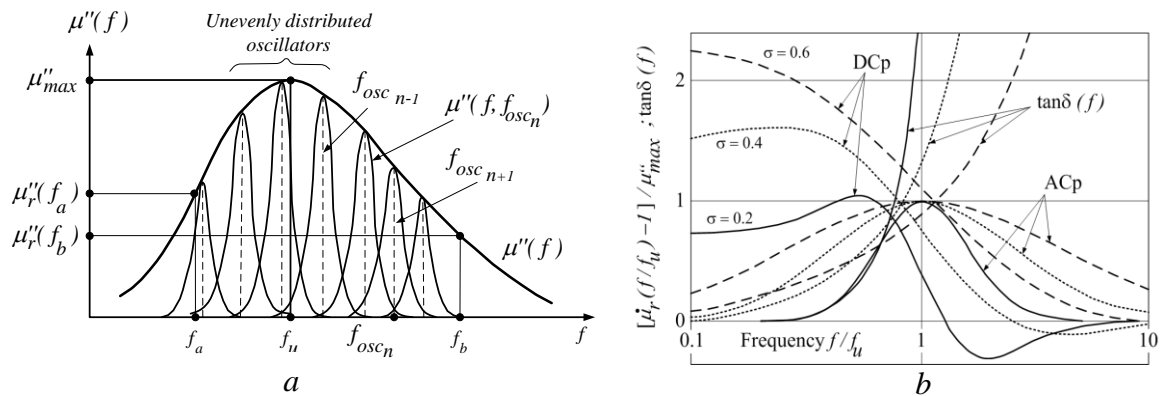


Figure 2.8 a) Inhomogeneous widening of ACp; b) normalized symmetrical CIP spectra for three σ values, eq. (2.14), DCp part is obtained by the use of KKR (3.1);

Also it is assumed that the relationships for magnetization processes in the elementary volumes, the grains as a function of D , are similar to those which can be deduced from the analysis of experimental data of a variety of PF samples in relation to their average grain size D_a . Thus, in relation to D_a IQG exhibit clear correlations: linearity and obeys the modified Snoek's law [31]:

$$\mu(0) - 1 = C_1 D_a; \quad (2.12)$$

$$\mu''_{max} f_u D_a / M_s = 2\pi / \sigma, \quad (2.13)$$

where C_1 – const.; hence ferrites from IQG are the most appropriate for theoretical analysis. In contradistinction, for ferrites from TQG such a clarity is lost – linearity (if at all) needs to

be related to some effective grain D_{eff} and only the standard Snoek's law is fulfilled: $\mu(0) - 1 = C'_1 D_{eff}$ and $\mu''_{max} f_u / M_s = C'_2$, where C'_1 and C'_2 – const. In fact, these equations are used for true intrinsic and intrinsic samples respectively for dealing with their inner processes – ones in current grains D within PF samples.

From the previously mentioned interpretations, specifically (2.12, 2.13), it emerges that for IQG ferrite samples there is a distribution not only of sizes D , but of related frequency response of elementary volumes too (Fig. 2.8, a). The response is expected to arise from DW resonating at frequency f_{ODW} , $f_{ODW} \propto 1/D^2$, setting up the static permeability of current grain $\mu_G(0) \propto D$, (that comes about from DW pinned only on the grain boundary – as in the model of Globus [21]).

The statistical averaging of ACp of permeability of grains (described further in [28] for IQG ferrites and for TQG ferrites in [30]) allows ACp of CIP of the sample (as InP) to be obtained as:

$$\mu''(f) = \mu''_{max} \exp[-(\log f - \log f_u)^2 / 2\sigma^2] \quad (2.14)$$

where μ''_{max} and f_u , Fig. 2.8, a, characterize the absorption maximum of $\mu''(f)$; but $\sigma = 2\sigma_{log}$ for IQG and $\sigma = \sigma_{log}$ for TQG. The relation for $\mu''(f)$ with three parameters of ACp: μ''_{max} , f_u , and σ represents the symmetrical MS (along $\log f$ axis from the $\mu''(f)$ standpoint, Fig. 2.8, a).

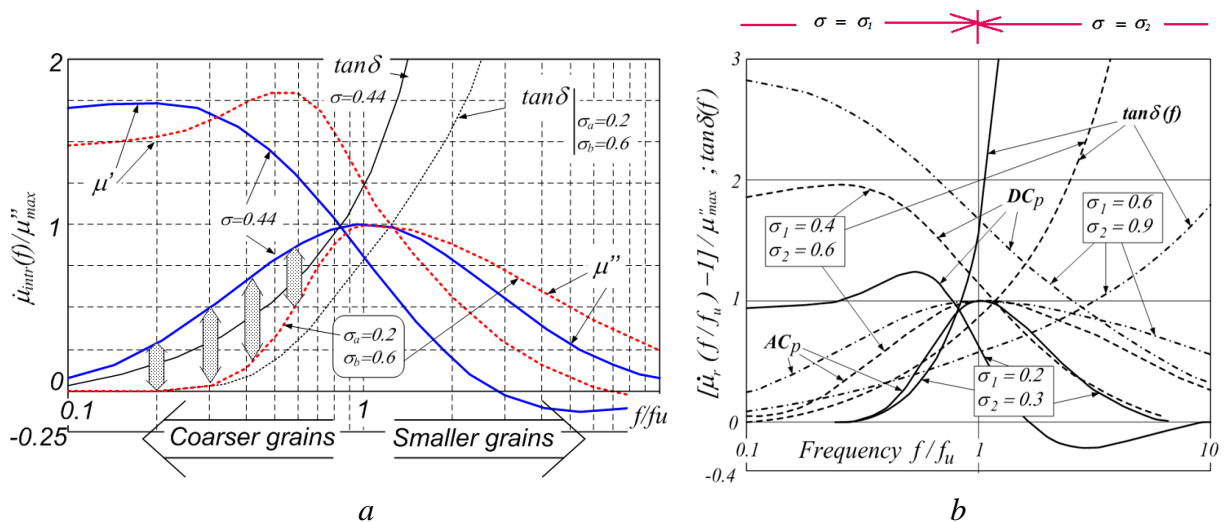


Figure. 2.9 a) Potential possibilities of the model to transform from symmetrical to asymmetrical type of spectra [32] b) Normalized asymmetrical CIP spectra for different σ_a and σ_b values, Eq. (2.14), DCp part is obtained by the use of KKR (3.1), [28]

The potential of Eq. 2.14 to present MS (for different values of σ) as normalized curves is shown in Fig 2.8, b: it can be seen that the change of σ (which in reality means the change of grain distribution) principally allows the process from a mainly relaxation type of

spectra ($\sigma = 0.6$) to a clearly resonant one ($\sigma = 0.2$), having the transition (between resonance/relaxation) value near 0.5 (in the process the dispersion components DCp were calculated by the use of KKR). For approximation of definite experimental spectrum, $\mu''_{exp}(f)$, with Eq. 2.14, the value of σ must be specified. In this case it can be requested, that experimental spectrum and its theoretical approximation would be equal at some frequency $f_a \neq f_u$. The fulfillment of these conditions results in equation (where frequency $f_a < f_u$ or $f_a > f_u$):

$$\sigma = |\log(f_u/f_a)| / \sqrt{2 \ln[\mu''_{max}/\mu''(f_a)]} \quad (2.15)$$

Even so, analysis of published experimental CIP spectra shows, that the majority of experimental MS show asymmetrical absorption curves $\mu''(f)$. In [31] it was shown that the reason for this comes from intragrain defects which in real PF appear in coarser grains cause extra pinning of DW. So, instead of one low resonant frequency of DW (when it is pinned only at grain boundaries) there develop several higher frequencies from resonating fragments of pinned DW; accordingly, ACp of CIP at lower frequencies decreases because of this pinning (Fig. 2.9, a), and the spectrum goes asymmetric and more resonant. For the analytical presentation of asymmetrical MS it is possible to use Eq. 2.14 as well, with two values of σ : one, σ_a for $f < f_u$ and another, σ_b for $f > f_u$. Corresponding frequency dependences in the thus modified Eq. 2.14, in normalized form, for several combinations of σ_a and σ_b (naturally $\sigma_a < \sigma_b$) are shown in Fig. 2.9, b – they realistically depict the most typical features of experimental MS. There is clearly seen from Fig. 2.9, b, that with $\sigma_a < 0.5$ values the DCp resonance attributes are appearing at frequencies $f < f_u$ and using the second σ_b value, that is higher than 0.5 – we can make more relaxant DCp character at $f > f_u$. Thus, we can construct the spectra close to experimental spectra form both with relaxation and resonance attributes (Fig. 2.9, b).

The modeling of magnetic spectra by taking account of PF microstructure offers the physical background for microstructure dependence of not only static magnetic permeability, but of complex magnetic permeability too. Included in the model assumption that DW are low loss resonators, offers universality: narrow distribution of grains ($\sigma < \sigma_B$) gives resonant type MS, but broad distribution ($\sigma > \sigma_B$) gives a relaxation type MS. Graphical representation of CIP spectra by means of microstructure parameters allows the conclusions to be made that: symmetrical spectra represent PF with rather perfect grains; asymmetrical spectra point to the presence of a considerable amount of intragrain defects.

2.2.5 Ferrites for SMPS

Switched mode power supplies (SMPS) provide the most efficient power conversion (the efficiency now reaches up to 97–98 % [57]). Due to the use of high switching frequency the construction of SMPS is compact and light. The actual problems here are noise filtering, electromagnetic interference (EMI) and radio frequency interference (RFI) suppression, which adds complexity to the construction. To reduce nonlinear influences on the power grid, power factor correction (PFC) is added to construction, which adds more complexity and cost to the SMPS. But all these requirements are needed to be in accordance with international standards [48, 67].

The majority of SMPS topologies are derived from the three non-isolated (without transformer) ones: buck (Fig. 2.10, a), boost (Fig. 2.10, b) and buck-boost. These topologies have the lowest component count (transistors, diodes, capacitors, inductors, etc.).

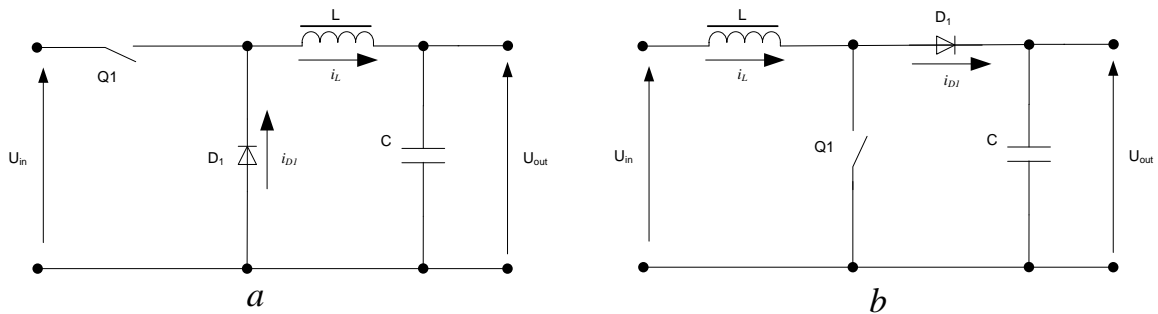


Figure 2.10. Simplified buck (a) and boost (b) converter topologies [48].

To extend the limits of non-isolated topologies the transformers are used. This provides input to output isolation; by varying the transformer turns ratio the duty cycle of a transformer can be optimized and peak currents flowing minimized; the multiple outputs can be easily achieved with multiple secondary windings and the polarity of the output can be selected by the choice of polarity of secondary versus primary winding. The disadvantage can be additional transformer size, weight and power loss.

The magnetic cores form an essential part of power supplies, and can be made from a great variety of materials and shapes, and can be classified into three main categories: tape wound cores, powder cores; and ferrites. Among them ferrites, having high resistivity, are common core materials for high frequency applications. The type of the core can be varied (Fig. 2.11). The most common choice for RF applications are toroidal cores [48] and have minimal leakage inductance in comparison to other core types (such as RM, P, EP, a. o.).

Common mode choke coils are used for suppression of common mode noise signals. It acts as a simple wire for differential mode signals, but produces high impedance for common

mode signals. The core material should be chosen from high permeability ferrite core, because the core would work in low fields and the needed inductance should be obtained with minimal turn amount. The use of magnetodielectrics is inexpedient due to low magnetic permeability and low cost of ferrites.

Differential noise is conducted on the signal line in one direction with the signal. This noise is suppressed by single or double wounded inductors installed on the signal line. Here, together with low amplitude noise, the high amplitude 50 Hz power supply current is present, which is equal to DC in these conditions. The core material can be chosen between ferrite cores with non magnetic gap or magnetodielectrc cores.

2.3 Review of ferrite HF problems.

The main problem in implementing a new design for magnetic related applications is to collect appropriate data on the materials that will be used [61–63, 66]. But, usually, provided information on ferrite core is based on low power measurements of small-sized toroidal cores, which is not always applicable. Larger cores of the same material can provide significant changes in material characteristics (see fig. 2.12). Therefore available information is incomplete for applications where such cores can be used. Furthermore, according to [61] the information provided in the design literature does not give solutions on how to deal with dimensional effects. The reality of this problem is easily noticeable in Figure 2.12 – with increased core size the absorption is greatly increased and dispersion has extremums over a greater extent; also the core working frequency range is lowered.

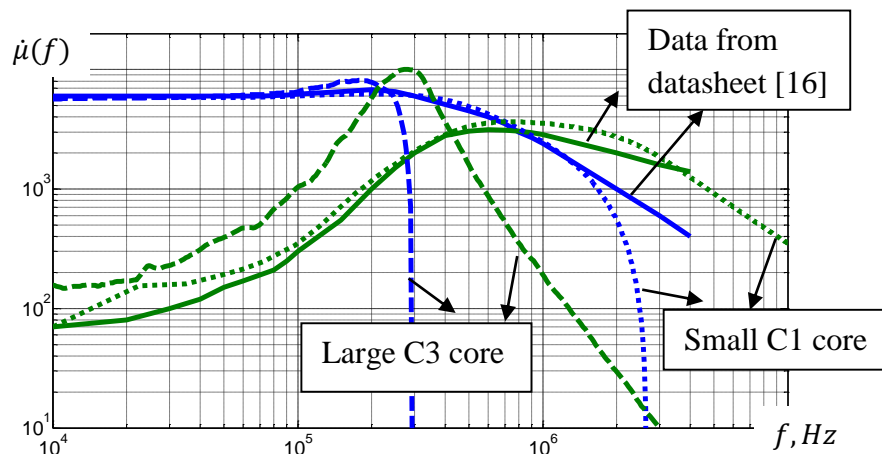


Figure 2.12 Measured and given [16] CMP for EPCOS T-35 material cores.

Newer-ending problems are related to the reduction of power losses of ferrites (especially MnZn ones) and increasing power supply efficiency [24]. Consequently, many new materials, that fulfill the demands of modern power supply designers, are studied and

developed [51]. But improvement of all ferrite characteristics cannot be achieved due to loss dependence from various factors (not only from the composition but from the microstructure too [24, 77], i. e. low frequency hysteresis loss depends on microstructure defects, porosity; the high frequency eddy-current loss can be decreased by higher electrical resistance of the grain boundaries and smaller size of the grains [77] etc.). But the grain size cannot be decreased indefinitely; in [24] it is stated, that for forward mode SMPS, core loss at 100 kHz switching frequency, increases if grain diameter is decreased below $6 \mu m$.

The miniaturization of SMPS is, mostly, achieved by increasing the switching frequency f_{SW} . But increased f_{SW} results in EMI problems. Decrease of EMI is possible to achieve both by traditional passive methods (filtering, shielding, grounding, proper PCB design, a. o.) and by active ones – spread spectrum technologies (SST) [69]

The analysis carried out in [38] shows that the improvement in EMC of the converter by use of SST yet produces an additional stresses on the components of output filter. For both components switching modulation generates extra power loss (as opposed to unmodulated case) which increases with the growth of frequency deviation $\pm \Delta f_{SW}$. During this more energy is dissipated just within $-\Delta f_{SW}$ than is saved (as against to f_{SW0}) within $+\Delta f_{SW}$. But this effect is not strong; it is possible to compensate it by slight increase of f_{SW0} and thus to maintain high efficiency of converter in the case of SST usage as well. Magnetic core can enter saturation due to the use of SST. This reflects as sharp increase in the power inductor current and consequently increase losses in the inductor. So when designing FM converter minimum switching frequency should be chosen properly to avoid core saturation.

As a consequence, it is believed that the study of CIP frequency spectra in relation to their MST may contribute to a better understanding of the magnetization processes of PF, eventually resulting in a better representation of frequency dependencies and more effective application of PF.

3 KRAMERS-KRONIG RELATIONS APPLICATION TO EXPERIMENTAL DATA

The Kramers-Kronig relations (KKR) relate the real and imaginary parts of a complex analytic function. The relations are used to calculate the real part of a characteristic from the imaginary part,– and vice versa. Eq. (3.1) and (3.2) describe the interrelationship of the real and imaginary parts of CIP:

$$\mu'(f) - 1 = \frac{2}{\pi} \int_0^{\infty} \frac{x\mu''(x)}{x^2 - f^2} dx, \quad (3.1)$$

$$\mu''(f) = -\frac{2}{\pi} f \int_0^{\infty} \frac{\mu'(x)}{x^2 - f^2} dx. \quad (3.2)$$

The integration has an infinite upper bound, but for actual components of CIP we may operate within finite boundaries e. g., (from frequency $f_A = 0$ to f_B , beyond which ACp is zero. For experimental

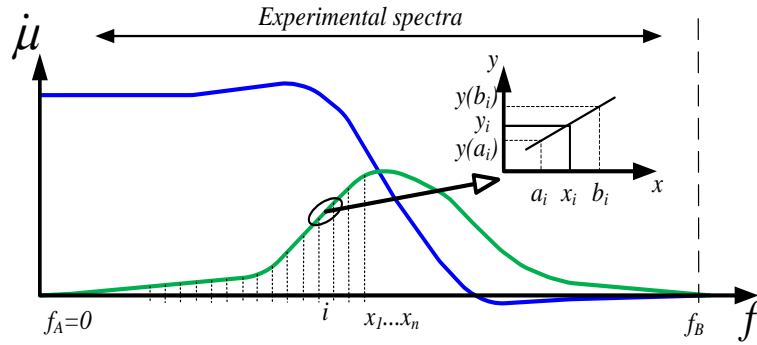


Figure 3.1. Kramers-Kronig application to measured CIP

results it is more convenient to replace the integration sign with summation, so the derived form of K-K relations than is:

$$\mu'(f) - 1 = \frac{2}{\pi} \sum_i \left(m_i (b_i - a_i) - \frac{m_i f}{2} \ln \frac{|f - a_i|(b_i + f)}{(f + a_i)|b_i - f|} + \frac{c_i}{2} \ln \frac{|b_i^2 - f^2|}{|f^2 - a_i^2|} \right); \quad (3.3)$$

$$\mu''(f) = \frac{2}{\pi} \sum_i \left(-\frac{m_i f}{2} \ln \frac{|b_i^2 - f^2|}{|f^2 - a_i^2|} + \frac{c_i}{2} \ln \frac{|f - a_i|(b_i + f)}{(f + a_i)|b_i - f|} \right), \quad (3.4)$$

where: $m_i = \frac{y(b_i) - y(a_i)}{b_i - a_i}$; and $c_i = \frac{y(a_i)b_i - y(b_i)a_i}{b_i + a_i}$ are the approximation coefficients determined directly from CIP curve (Fig. 3.1).

3.1 Magnetic spectra quality – analysis from KKR viewpoint

Often, the experimental magnetic spectra is doubtful, or of insufficient quality. In [80] it is suggested to use the Kramers-Kronig relations as a proper mathematical instrument for evaluating the doubtful magnetic spectra. For example the spectra presented by Dok Won Lee a. o. in [45, Fig. 1, Fig. 2, Fig. 3] is noisy at lower frequencies (from 1 to ~ 50 MHz), so it is hard to find the correct value. The application of Kramers-Kronig relations (green dashed line) to above mentioned permeability curves (blue solid line) reveals the true values for

inaccurate, noisy data, and also provided information that measured in [45, Fig. 1] permeability data is inaccurate (Fig. 3.2, a).

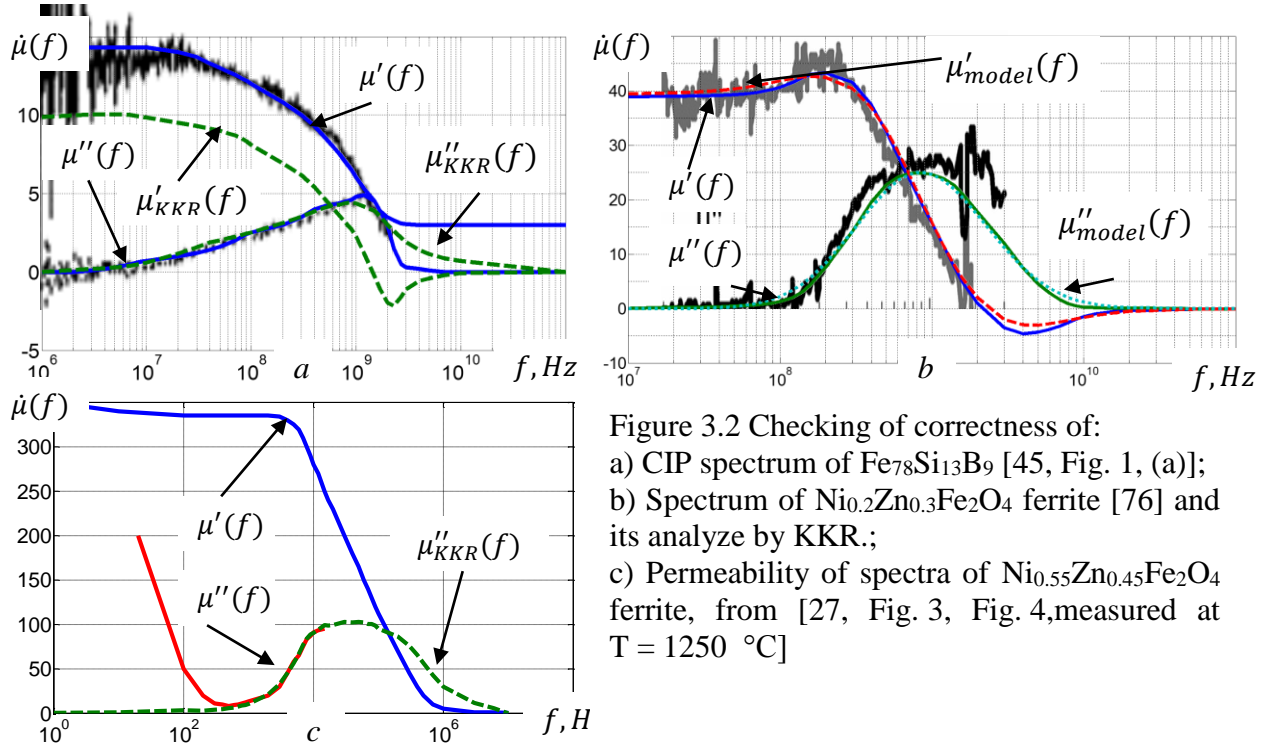


Figure 3.2 Checking of correctness of:
a) CIP spectrum of $\text{Fe}_{78}\text{Si}_{13}\text{B}_9$ [45, Fig. 1, (a)];
b) Spectrum of $\text{Ni}_{0.2}\text{Zn}_{0.3}\text{Fe}_2\text{O}_4$ ferrite [76] and its analyze by KKR.;
c) Permeability of spectra of $\text{Ni}_{0.55}\text{Zn}_{0.45}\text{Fe}_2\text{O}_4$ ferrite, from [27, Fig. 3, Fig. 4, measured at $T = 1250^\circ\text{C}$]

The use of KKR for evaluation of doubtful (noisy) data is also shown in Fig. 3.2, b. Provided in [76] CIP spectrum of $\text{Ni}_{0.2}\text{Zn}_{0.3}\text{Fe}_2\text{O}_4$ ferrite films is rather noisy and it is cut off between $2 \times 10^7 < f < 3 \times 10^9 \text{ Hz}$. Thus, for correct evaluation of this spectrum, ACp was prolonged from both sides till zero. The slope of right side was chosen so, that after performing KKR evaluation, calculated DCp part slope ($3 \times 10^8 < f < 2 \times 10^9 \text{ Hz}$) will be same as experimental one. The analysis showed, that data provided up until 2 GHz is reliable, nevertheless it is not full.

The other publication, provided by Islam R. [27], presented the confusing data on $\text{Ni}_{0.55}\text{Zn}_{0.45}\text{Fe}_2\text{O}_4$ ferrite CIP spectra measured within different temperatures. According to [27, Fig. 4, Fig. 3] – ACp has pronounced increase of amplitude at lower frequencies (red curve in Fig. 3.2, c), but the DCp does not represent any resonance attributes at these frequencies, instead – stays const. The analysis of these curves with help of Kramers-Kronig relations proved the incorrectness of the experimental ACp low frequency data. For correct evaluation of this spectrum with KKR, DCp part was prolonged till 5 MHz. Even in this case the application of Kramers-Kronig relations on experimental data provides information on quality of measured data, points to confusing results and helps to estimate doubtful, noisy data.

3.2 Decomposition of spectra

By the use of Kramers-Kronig relations we can get the data, that is hard to measure directly. For example: The spectra measured by J. Slama, et. all. in [64], represents ACp with two resonances: domain wall resonance at $f \approx 90$ MHz and spin resonance at $f \approx 160$ MHz.

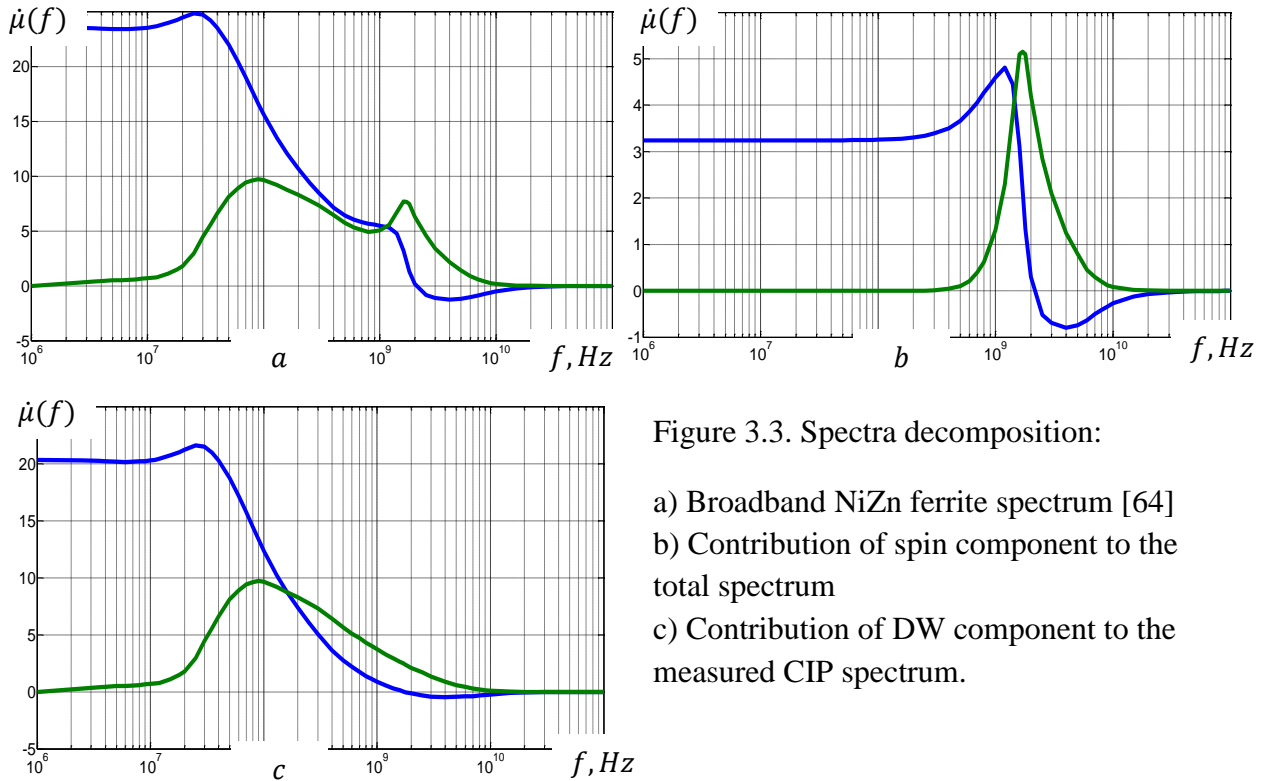


Figure 3.3. Spectra decomposition:

- a) Broadband NiZn ferrite spectrum [64]
- b) Contribution of spin component to the total spectrum
- c) Contribution of DW component to the measured CIP spectrum.

The results of spectra decomposition showed, that:

- it is possible to distinguish for the contribution of DW and NSR components to whole spectrum;
- real values of ACp maximums and corresponding frequencies can be precised with decomposition (e. g. in case of close DW and NSR absorptions localization)

Thus, the decomposition of spectra into components allows to estimate the component contribution to CIP, which is hard to measure directly. Also, using inverse process (as it is showed in Fig. 6.1) we can estimate missed component contribution (in this case the NSR) on the whole spectrum and thus evaluate measured spectra quality. The study of this low permeability spectrum (Fig. 3.3) proves, that contribution of NSR part to $\mu(0)$ is less than 20 % (in the case of high permeability CIP spectrum, the NSR contribution is even less, in some cases it can be ignored, e. g., fig. 2.2).

4 STUDY OF MICROSTRUCTURE OF SAMPLES USED; MST ASPECTS FOR PF OF SMPS

Mathematical statistical methods are used for describing of microstructure parameters of PF [42, 56]; there can be defined mean arithmetical value, standard deviation, dispersion and others. The most complete characterization can be achieved with probability density distribution function of these parameters or values. Microstructure can be characterized by mean grain diameter or distribution dispersion. The experiments prove that grain diameters have log-normal distribution function [79], and from this function we can easily determine the statistical parameters of MST.

4.1 Statistical parameters of ferrite microstructure

MST parameter characterization of studied samples was made by use of Saltikov's [56, 59] method. This method is based on stereo metric relations, that can describe grain distribution in three-dimensional space by using of micrographs. Thus we need to decrypt the micrograph, in order to obtain statistical MST parameters: \bar{D} – average diameter of grain, $\sigma(D)$ – standard deviation of grain diameter and $\sigma(\ln D)$ standard deviation of $\ln D$. To obtain reliable results for microstructure parameters the micrographs were taken from different parts of sample.

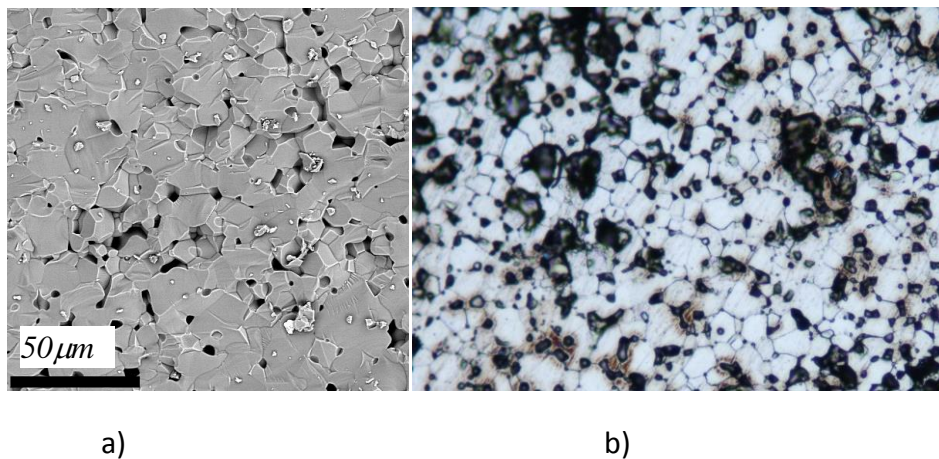


Fig.4.1. Micrographs for MnZn ferrite (6000HM-1): a) – scanning electronic microscope (SEM) image, b) – etched surface.

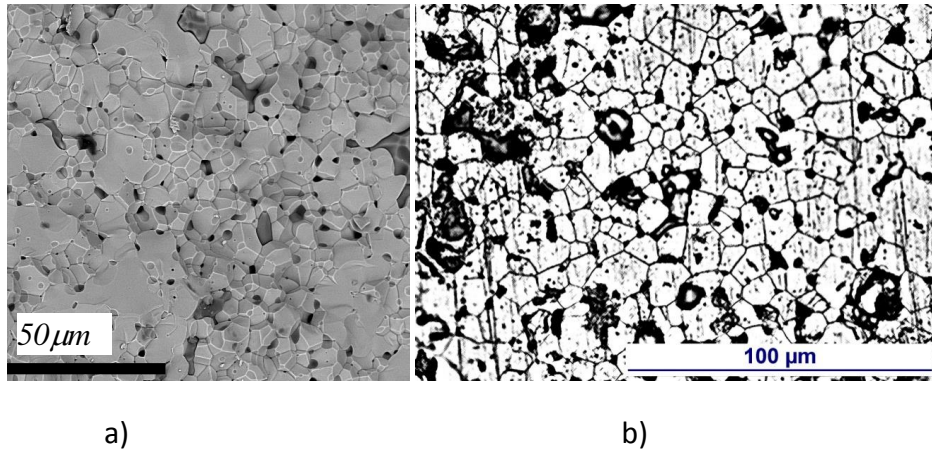


Fig. 4.2. Micrographs for MnZn ferrite (T37): a) – SEM image, b) – etched surface.

As we can see from Figs. 4.1–4.3 it is hard to obtain excellent quality of polished surface due to crumbled grains and pores. The micrograph decryption is based on finding amount, dimensions of crumbled grains and pores. Then we can construct the lognormal distribution function:

$$N_i = \frac{N\Delta}{\sqrt{2\pi}D_i\sigma(\ln D)} e^{-\left(\frac{(\ln D_i - \overline{\ln D})^2}{2\sigma^2(\ln D)}\right)}, \quad (2.1)$$

where $\overline{\ln D}$ – grain diameter average logarithm, $\sigma(\ln D)$ – standard deviation of $\ln D$, $\sigma(D)$ – standard deviation of grain diameter, N – the number of grain D in one volume.

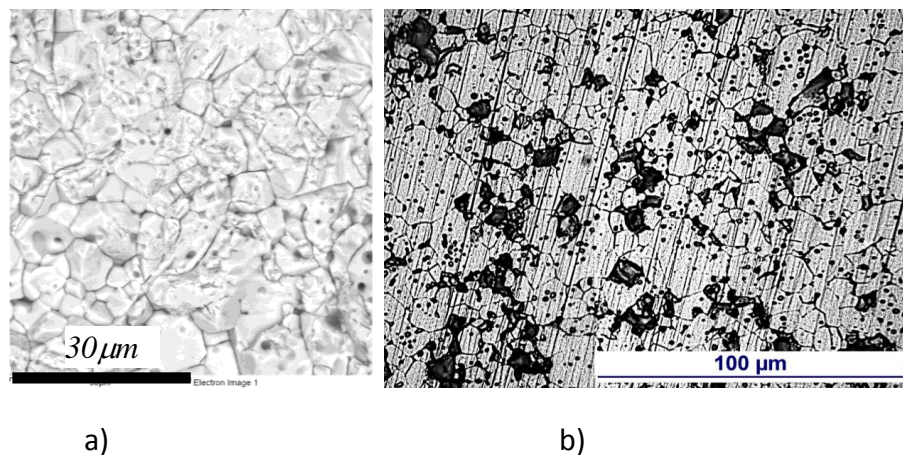


Fig.4.3. Micrographs for NiZn ferrite: a) – SEM image, b) – etched surface.

The obtained data shows that microstructure – aggregation of polycrystal grains is that of normal grain growth for all of the ferrite samples (because $\sigma_{\ln D}$ tend to 0.5 as it is for MST

with lognormal grain distribution [28, 42]). Nevertheless, there is clearly noticeable from micrographs, that all of ferrites have defects within numerous of grains.

4.2 Preparing of samples with similar microstructure

For the research of CIP of the samples we need to make series of experiments on each researched ferrite group. The quality of MST of samples points to quality of material.

In the following investigations of correlation of MST and CIP spectra it is proposed to resolve two problems:

- 1) correlation of definite CIP spectrum with the MST of sample;
- 2) dependence of CIP spectra on different geometric dimensions under fixed MST.

In the first case we can use PF cores of conventional technology, with measured CIP and analyzed MST.

In the second case there is need for samples of similar composition and MST but of different geometries. To fulfill this ferrite cores should be cutted off from the same ferrite tile, that had same preparing and sintering conditions within whole tile area. Therefore tested ferrite cores were cut off from ferrite tiles with waterjet technique. Waterjet cutting was selected due to it benefits of other techniques (mechanical, laser or plasma cutting) [39, 71, 70]: cutting is performed without overheating, width of the cut (kerf) is relatively thin, which minimizes the loss of material, can make every desired form of core. The only problem of this method is to find the water jet pressure level high enough to cut through ferrite tile, but not to break the material.

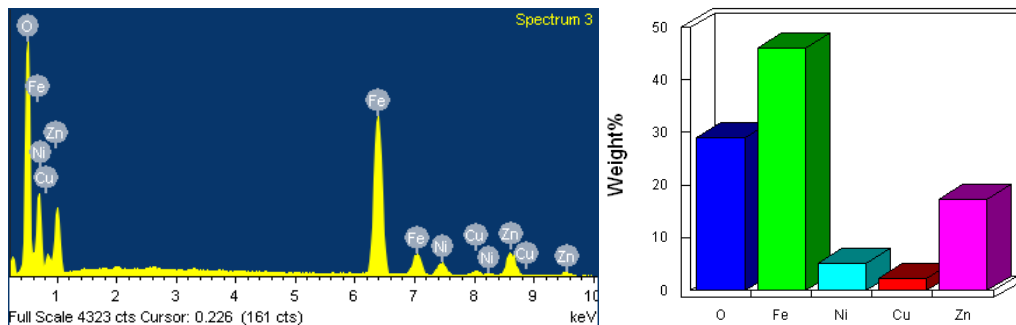


Figure 4.4. Elemental analysis of NiZn samples [34]

There were produced two groups of ferrite cores with different inner/outer diameter (ID/OD) for experiments. First group is cut off from Ferroxcube 4S60 ferrite tiles, second group is cut off from Nevaferit – 6000HM-1 ferrite tiles. The elemental analysis of the cutted ferrites (Fig. 4.4, 4.5) did not reveal any contamination. The geometrical and statistical parameters of all studied ferrites are collated in table 4.1.

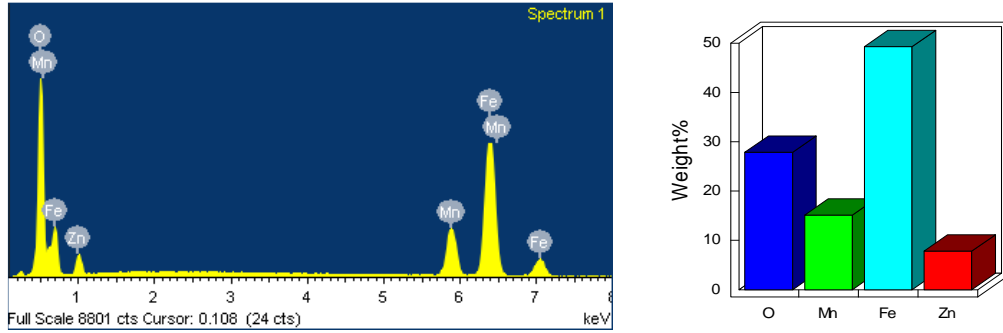


Figure 4.5. Elemental analysis of MnZn samples [34]

Table 4.1. Studied sample geometrical and statistical parameters

Group	N ₀	Dimensions, mm	A, mm ²	$\mu(0)$	$\mu(0)_{exp}$	D, μm	σ_{lnD}
NiZn, 4S60	A1	R12 × 8 × 6	12	2000	2200	7.9	0.55
	A2	R20 × 10 × 6	30	2000	2100	7.9	0.55
	A3	R31.5 × 20.5 × 6	33	2000	2125	7.9	0.55
	A4	R40 × 23.5 × 6	51	2000	2140	7.9	0.55
MnZn, 6000HM1	B1	R10 × 4.3 × 10	28.5	6000	6750	12.9	0.53
	B2	R20 × 9.1 × 10	54.5	6000	6530	12.9	0.53
	B3	R25 × 12 × 10	65	6000	6650	12.9	0.53
	B4	R30 × 14.3 × 10	78.5	6000	6850	12.9	0.53
	B5	R33 × 10 × 10	115	6000	5523	12.9	0.53

The obtained data shows that microstructure – aggregation of polycrystal grains is that of normal grain growth for all of the ferrite samples (with $\sigma(\ln D) \approx 0.5$). There is clearly noticeable, from micrographs, that all of ferrites have defects within numerous of grains, which leads to CIP asymmetry.

5 MEASUREMENTS OF FERRITE MAGNETIC AND DIELECTRIC PROPERTIES

In our CIP measurements we use toroidal ferrite samples with one layered evenly placed windings. We use different approaches and methods to obtain CIP data. For lower frequencies (up to 2 MHz) we use specialized measurers (e. g. Q-meters, phase meters, LRC bridges, etc.) in coup with vector network analyzer (VNA ZVR-E) help [1, 2], for higher frequencies we use ZVR-E with shortened coaxial line connection support [80] (our VNA ZVR-E has the frequency range from 9 kHz up to 4 GHz). From many experimental data measured there is an agreement between the results obtained with different measuring methods. To deal with slight noise there was done a shielded ferrite connection to ZVR-E, with possibility to connect ferrite both to one or two ports. CIP can be constructed by measuring complex value of S11, S12, S21, S22 parameters for two ports and then moving to Z parameters to obtain complex impedance value \dot{Z}_{in} from them.

$$\dot{Z}_{in} = \dot{Z}_{11} - \frac{\dot{Z}_{12}\dot{Z}_{21}}{\dot{Z}_{22}+Z_0}, \quad (5.1)$$

where $Z_0 = 50\Omega$ is characteristic impedance of test port. Then CIP of a sample

$$\dot{\mu}(f) = 1 + \frac{\dot{Z}_{in}}{j2\pi f L_0}, \quad (5.2)$$

where L_0 – inductance without magnetic sample.

The main principle of measurement with phase meters is that we need to hold same output voltage level within all measurement frequency range. Knowing voltage before sample (U_{in} , source voltage), voltage after the sample (U_{out} , voltage on known output load R), phase shift between these two voltages and by using following equations [80]:

$$\mu' = L/L_0 = \frac{U_{in}R\sin(\varphi)}{U_{out}\omega L_0}, \quad \mu'' = R_m/\omega L_0 = \frac{U_{in}R\cos(\varphi) - U_{out}R}{U_{out}\omega L_0}. \quad (5.3)$$

Thus we can construct CIP spectrum with help of phase meter.

5.1 Experimental results

The CIP was measured for all studied ferrites, the ferrites were divided into three groups: A, B, C. The results are representing CIP dependence of frequency, and the following analysis from MST too.

As it is seen (Fig. 5.1, a–c) – for samples A1...A4 with similar MST there is no real difference in CIP in dependence of size of the core. From the measurement results of MnZn B1...B5 samples with similar MST (Fig. 5.1, b) it is seen that, ACp maximum of CIP became dependent on frequency (samples B1...B4, the bigger the core size – the lower the ACp

maximum frequency), and, in case of pronounced resonant character of sample B5 – dimensional resonance conditions obviously were met.

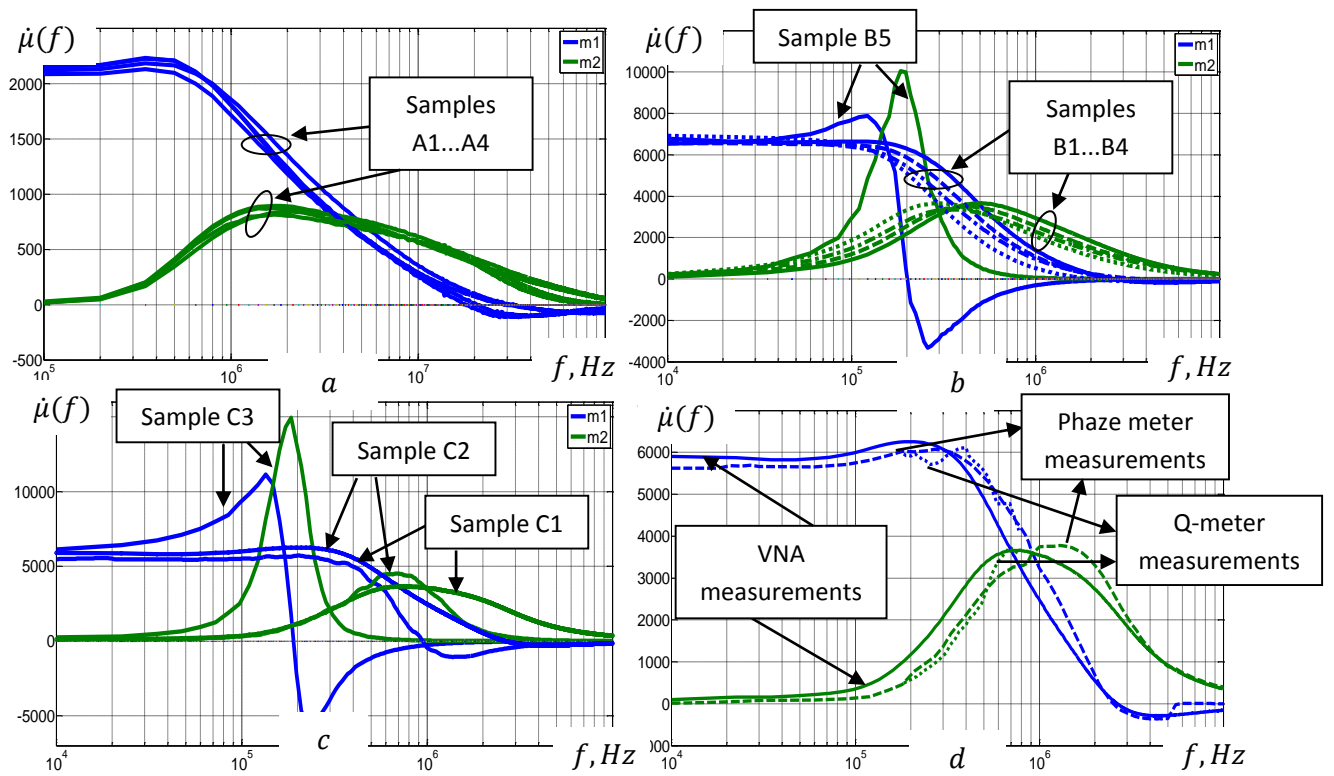


Figure 5.1. Measured CIP of a) samples A1..A4, b) samples B1..B5, c) samples C1..C3 (m1, m2 stands for $\mu'(f)$ and $\mu''(f)$), d) VNA measurement comparison with classical methods.

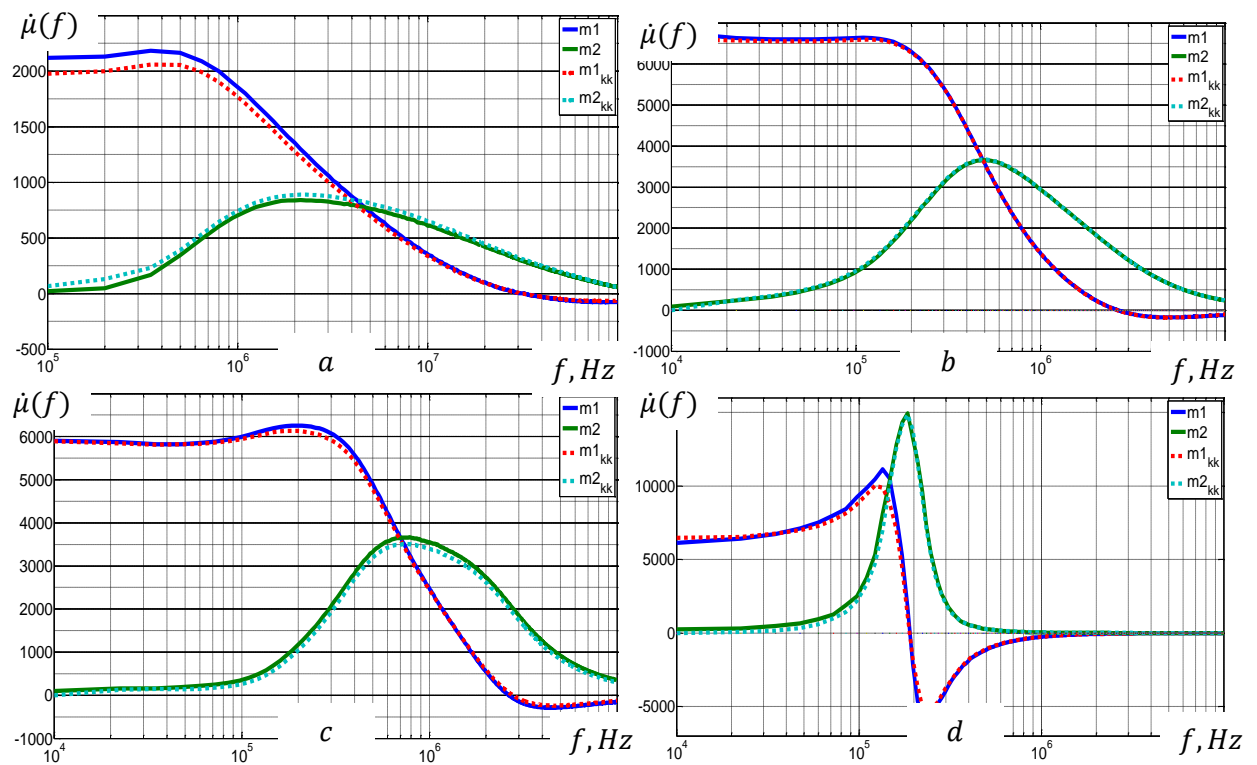


Figure 5.2. KKR application to a) A1 sample, b) B1 sample, c) C1 sample, d) C3 sample.

The results for C1...C3 (commercial MnZn samples) proves, that dimensional resonance highly influence the CIP of ferrite core: with the growths of dimensions of the core, the DR becomes more pronounced and the ACp maximum frequency decreases.

For the verification of VNA measurements results there are used classical Q-meter and phase meter measurements. In order to compare measured data there is used KSC of C1 sample (Fig. 5.1, d). As it is seen from Fig. 5.1, d, data obtained from VNA and phase meter measurements are in good correlation. The data obtained with Q-meter has good correlation only within lower frequencies (the AF data is not precise due to parasitic parameters).

The quality of the obtained experimental data was tested with KKR (Fig. 5.2, where m1 and m2 stands for experimental $\mu'(f)$ and $\mu''(f)$ data; m1kk and m2kk stands for KKR evaluation of $\mu'(f)$ and $\mu''(f)$) and showed good correlation. This proves that measurements are performed correctly and experimental data can be used for spectra interpretations.

5.2 Complex permittivity measurements

The experimental measurements of complex permittivity $\hat{\epsilon}_r(f)$ were performed on ferrite samples (cut from corresponding ferrite ring cores). On the polished surface of these samples were sputtered thin copper electrodes (Table 5.1).

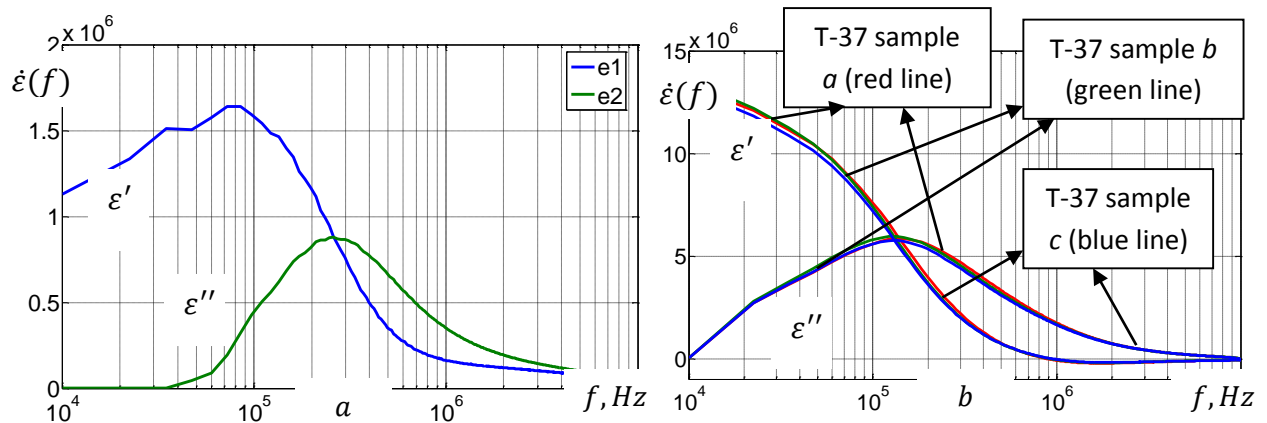


Figure 5.3 Measured complex permittivity of a) 6000HM-1 MnZn ferrite (e1 stands for ϵ' and e2 stands for ϵ''); b) measured complex permittivity of T-37 MnZn ferrite.

Table 5.1. Sample parameters for complex permittivity measurements

Material	Sample size, mm	Metallization area, mm	$\epsilon_r(0)$
6000HM-1	11 × 11 × 2	8.5 × 9	1.6 × 10 ⁶
T-37 <i>a</i>	16 × 8 × 1.1	4 × 9.6	13.3 × 10 ⁶
T-37 <i>b</i>	16 × 8 × 0.9	3.5 × 9.5	13.5 × 10 ⁶
T-37 <i>c</i>	16 × 8 × 0.8	4 × 7	13.1 × 10 ⁶

The results showed, that studied MnZn ferrites have high value of permittivity, thus the conditions for DR can be realized.

6 STUDY OF CORRELATION BETWEEN THE MODELING AND EXPERIMENTAL MS

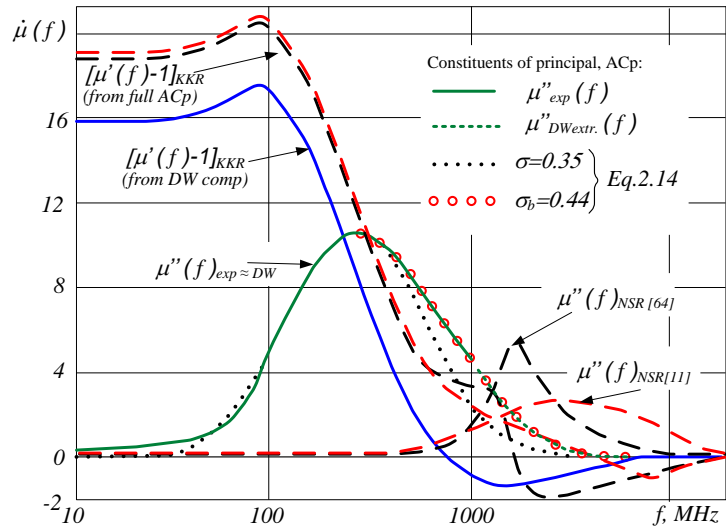
For the proof of the practical validity of Eq. 2.14 for definite MS it should be recalled that the modeling initially was developed for samples from IQG and later on modified for TQG ferrites as well at frequencies corresponding to large amplitude (domain wall) dispersion region. For the detailed analysis of correctness of the model there are used a great number of various CIP spectra both measured by us on our samples and from international scientific publications, as well (from the large general collection of PF with different compositions we first use two types of internationally widely studied ferrites: yttrium-iron garnet (YIG) and nickel (NiFe_2O_4) [58] ferrites).

6.1 Investigation of symmetrical spectra of CIP

Since there are practically no symmetrical MS within the group of mentioned nickel ferrites we are searching for the one most close to symmetrical. Such samples to check Eq. 2.14 should be searched among those PF sintered at relatively low temperatures (in order to avoid defects in the grains [20] that is one of starting prerequisites of the model). A large body of such samples were produced by A. Globus' method [20–23]; nevertheless some asymmetry do occur in their ACp of CIP spectra as well (thus evidencing of the existence of at least few defects in grains however). Even so at this moment these are the best available representatives. In the following, as the experimental prototype of $\mu_{exp}(f)$ from the set of curves is taken the most broadband ACp with relative small asymmetry (Fig. 6.1) of NiFe_2O_4 ferrite from [20, a] (having $D_a = 1.8 \mu\text{m}$ and ACp measured within $0.01...1 \text{ GHz}$). For verification of quality of this spectrum by KKR, there is need of full absorption spectrum. Hence, it is extended beyond 1 GHz, additionally adding next typical – natural spin resonance region (NSR) dispersion component to experimental $\mu_{exp}''(f)$ one (Fig. 6.1). NSR components ($\mu''(f)_{NSR}$) are extracted from two recent publication data [64, Fig. 2] and [11, Fig. 3.1]) by decomposition of corresponding spectra. Such a composed spectrum gives, using KKR and either of two mentioned $\mu''(f)_{NSR}$ almost the same value of $\mu(0) - 1$ and $\mu'(f)$ differing from experimental values only near NSR region. So it is possible to assume that $\mu''(f)$ as DW component is measured (for $f \leq 1 \text{ GHz}$) and continued properly (for $f \geq 1 \text{ GHz}$) and can be used to examine (2.14).

Estimation based on (2.14) for ascending part of $\mu''_{DW}(f)$ gives $\sigma = 0.35$; this allows for symmetrical spectrum (Fig. 6.1, dotted) that noticeably differs from $\mu''_{DW}(f)$ only at HF.

If there are used $\sigma_a = \sigma$ and $\sigma_b = 0.44$ (for descending part of $\mu''_{DW}(f)$) then approximation correlates well along the whole $\mu''_{DW}(f)$ curve. Thus in this case of rather small asymmetry of spectrum the values of σ differ slightly: $\sigma_a = 0.35$ and $\sigma_b = 0.44$; the use of them now allows to cover the whole ACp



(with very close approximation both for ascending and descending parts of ACp, Fig. 6.1). The values of σ_a and σ_b regardless of publication authors' claim of this PF to be of PFI type, nevertheless show that obviously there are few defects in coarser grains. This means that value of σ_a is slightly less, but σ_b – higher than that of true PFI. Because the asymmetry of this spectrum is small, presumably the true picture may be characterized by the average dispersion $\sigma_{av} = (\sigma_a + \sigma_b)/2 = 0.4$; the use of (2.11*) in this case gives the value for grain's distribution $\sigma_{lnD} = 0.46$ and this value thus tells that MST of PF under study is really close to normal one (since in [42], for normal MST was developed the criterion: $\sigma_{lnD} \approx 0.5$).

6.2 Application of the model for presentation of asymmetrical spectra

As it was mentioned before, real experimental CIP spectra almost without exceptions are asymmetrical ones. Analysis of possibilities of their presentation are based on the modified model (§ 2.2.4), firstly, on the ground of experimental data for nickel ferrite from different international publications (§ 6.2.1); later on there are added data following from our samples.

6.2.1 Presentation of CIP spectra of nickel ferrites.

If to similar analysis (as it was with symmetrical spectra) is subjected another nickel PF sample of the same composition as before [64] (Fig. 6.2 a), but apparently tending to TQG

because of rather pronounced asymmetric character of CIP, then it is possible to get the following data: $\sigma_a = 0.35$ $\sigma_b = 0.79$, $\sigma_{av} = 0.57$ (Fig. 6.2 a).

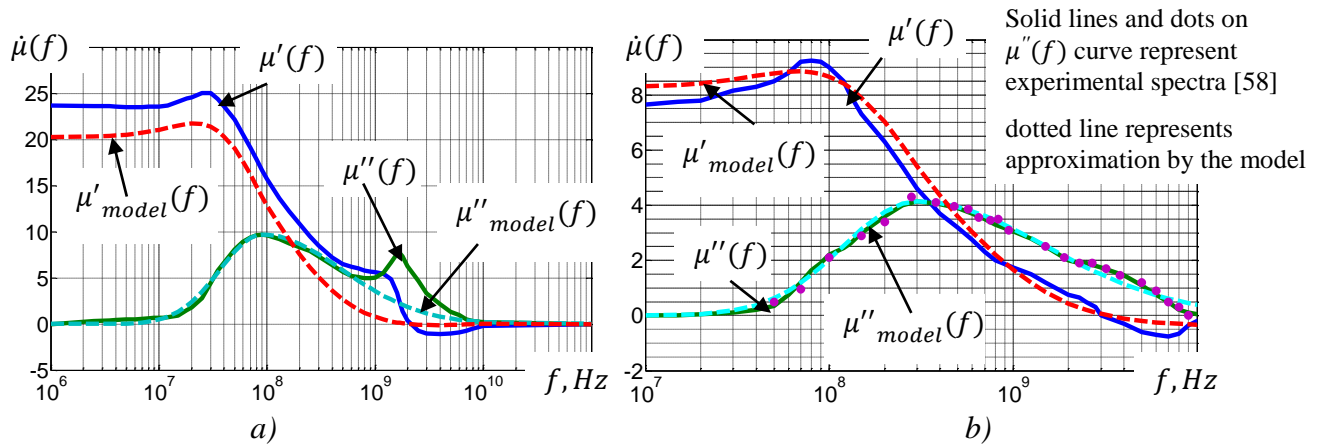


Figure 6.2. Application of the model to a) broadband NiFe₂O₄-ferrite spectrum [60]; b) magnetic spectrum of NiFe₂O₄ ferrite [58]

The character of DCp as DW one (Fig 6.2 a; $\mu'_{model}(f)$ obtained by the use of KKR) replicates correctly the measured data (up to ~ 300 MHz) until the influence of NSR component becomes significant, thus the application of the model to DW component is successful. The value of σ_{av} points to lower quality of MST of this PF as it was for ferrite with symmetrical spectrum.

In the case of another NiFe₂O₄ ferrite [58] (Fig. 6.2 b) the approximation by the model gives good correlation with the measured data on whole measured CIP range with the parameters: $\sigma_a = 0.42$ $\sigma_b = 0.68$, $\sigma_{av} = 0.55$. Obviously this ferrite is fine-grained one as to compared with precedingly analyzed samples (because of low value of $\mu(0)$ and high value of f_u). Nevertheless its MST characteristics are typical for common ceramic technology samples.

6.2.2 Presentation of CIP of samples with identical microstructure

Analysis of CIP of the above mentioned ferrites show that their spectra substantially depend on MST of definite sample. In the case of industrial grade samples their MST may vary considerably and so their spectra. In the event of similar MST the spectra as well should be similar. To prove this hypothesis (which, as well, can give additional confirmation for the model) we need the samples with similar MST.

In order to obtain the identical MST within the group of samples, we cut such samples of different inner/outer diameters (Tab. 6.1) from corresponding ferrite tiles (more details in § 4.2). In Fig. 6.3 (a) is shown MS of one representative from group (ring sample A1 of NiZn-ferrite Ferroxcube 4S60 measured by us). The application of the model firstly is used as

symmetrical approximation with one $\sigma = \sigma_a = 0.51$ value (Fig. 6.3 a, dotted curve), which shows, that spectra is asymmetrical: there is good correlation only within $f < f_u$ region. The use of $\sigma_b = 0.81$ for the values within $f > f_u$ provides good approximation for this region as well (Fig. 6.3 a, teal dotted line). Thus, ACp parameters: $\sigma_a = 0.51$ and $\sigma_b = 0.81$ allow for very close approximation of all curve but $\sigma_{av} = 0.66$ is rather high (micrograph in chapter 4, Fig. 4.5 b, indeed shows considerable amount of defects in grains, having $D_a \approx 7.5 \mu m$).

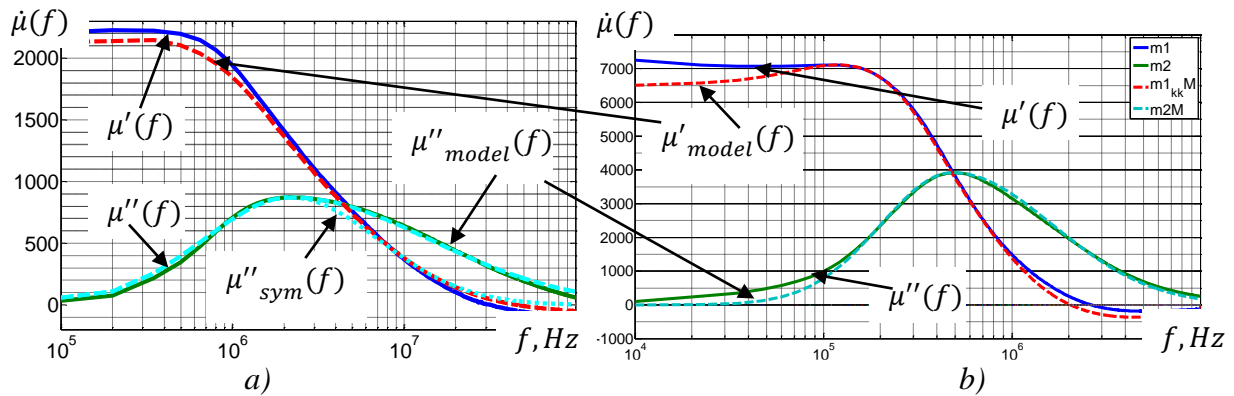


Figure 6.3. Spectrum of sample a) A1 and its approximations; b) B1 and its approximations.

Identical asymmetrical spectra are measured within this group of NiZn ferrite for other 3 samples with identical MST (Tab. 6.2, group A), and the values of the model are similar (Tab. 6.2). The σ_{av} value greater than 0.5 for this entire group allows for conclusion that MST of these samples are normal one but with defects, which is in agreement with micrographs (Chapter 4, Fig. 4.3). All this demonstrates that hypothesis about similar spectra in the case of similar MST is true at least in case of NiZn-ferrites.

To prove this hypothesis for MnZn-ferrites another group of ferrites (dimensions in Tab. 4.1) with the similar MST is produced and studied: group B – MnZn 6000HM-1 ferrite toroidal cores (Tab. 6.1). The application of the model to the one of samples – B1 is presented in Fig. 6.3 (b). The model parameters for B1 sample are $\sigma_a = 0.41$, $\sigma_b = 0.53$, $\sigma_{av} = 0.47$. The approximation showed good correlation with experimental data. Directly carried microstructure analysis provided $\sigma_{inD} = 0.53$ value, which is in good correlation with σ_{av} value. In principle it points to more or less normal microstructure, only with few intragrain defects. The micrograph provided by SEM (Chapter 4, Fig. 4.1, a) indeed show, that there is minimal amount of defects, but the porosity level still is considerable. Nevertheless the close correlation between the model parameters and that of microstructure indicates that assumption that large amplitude absorption region is determined by DW processes is truthful.

Table 6.1. Model parameters for studied ferrite cores.

Group	N_0	σ_{lnD}	σ_a	σ_b	σ_{av}	<i>The making of samples</i>
	A1	0.55	0.51	0.81	0.66	
NiZn, 4S60	A2	0.55	0.50	0.80	0.65	<i>Cutted from ferrite tile</i>
	A3	0.55	0.52	0.81	0.66	
	A4	0.55	0.52	0.84	0.68	
	B1	0.53	0.41	0.53	0.47	
MnZn, 6000HM1	B2	0.53	0.43	0.55	0.49	<i>Cutted from ferrite tile</i>
	B3	0.53	0.44	0.54	0.49	
	B4	0.53	0.44	0.57	0.50	
	B5	0.53	←	DR	→	
	C1	0.53	0.39	0.50	0.44	
MnZn, TDK T37	C2	0.52	←	DR	→	<i>Commercial products</i>
	C3	0.53	←	DR	→	

If we look at the spectra of another samples of this group (Fig. 6.3 b) than it is possible to notice that maximum of absorption f_u gradually shifts to lower frequencies with the growth of dimensions of the samples (Tab. 6.1). However the general view of spectra B1...B4 are similar and they are possible to approximate by nearly same parameters of the model: these parameters obviously still represent MST and its similarity. Contrary to this the spectrum of sample B5 (Fig. 6.3, b) is something else against just mentioned CIPs – it is pronouncedly resonant, near-symmetrical and narrow band – evidently the dimension resonance (DR, § 6.3) sets up, spectrum no longer is directly connected with MST. A small component of DR is probably the chief cause of shifts of f_u in samples B1...B4 as well.

6.3 Presentation of CIP of samples exhibiting dimensional resonance

The dimensional resonance phenomena is not well studied as well as the effects related to this phenomena (they are sometimes avoided for final calculations of SMPS magnetic components [61–63]). These effects often need to be obviated since they convert not only the spectrum of CIP (i. e., $\dot{\mu}_{int}(f)$ to $\dot{\mu}_{ext}(f)$) but can destroy devices by cracking or shattering magnetic core if excited at DR frequencies f_{DR} . Basing on DR theory [10, 61, 66], there are several conditions for the dimensional resonance in ferrites to occur:

- high permeability value
- high permittivity value

- one of the core cross-sectional dimensions must be comparable to half of the wavelength.

So, if the core dimensions are proportional to the half of a wave length the dimensional resonance can occur, and the wave length for a material with losses then is [66]:

$$\lambda/2 = \sqrt{(c_0^2/2f^2) / [|\mu||\varepsilon| + \mu'\varepsilon'(1 - \tan\delta_m \tan\delta_d)]} \quad (6.1)$$

where $c_0 = 1/\sqrt{\mu_0\varepsilon_0}$ – velocity of electromagnetic waves in vacuum. This means, that for ferrite cores, the wavelength is shortened, therefore the third criteria can be easily achieved.

Based on Eq. 6.1 and three defined conditions, taking typical for MnZn ferrites [66] $\varepsilon \approx 10^5$, and three different $\mu(0)$ values (2000, 5000, 10000) – we can construct DR appearance dependency from wavelength and frequency (Fig. 6.4). As it is seen – The DR resonant frequency becomes smaller for higher permeability ferrites. So for ferrite with $\mu = 5000$ and $L = 10$ mm the DR can occur at 1 MHz frequency. This means, that large MnZn cores cannot be used for HF applications [61, 66]. For reduction of the DR effect there is suggested [66] to use the non magnetic air gap in the ferrite core. Thus, the high permeability value is then lost. Another way – is to ensure, that that cross-sectional dimensions are much smaller that the half-wavelength obtained by Eq. 6.1.

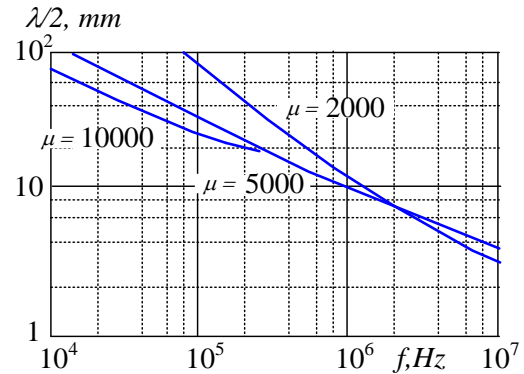


Figure 6.4 Dimensional resonance dependency from $\frac{\lambda}{2}$ and f [66].

For the experimental study of DR there firstly were selected industrially made toroidal high permeability (~ 6000) MnZn cores of TDK ferrite T37, with dimensions (in mm) $R12.5 \times 7.5 \times 5$, $R20 \times 10 \times 7$, $R40 \times 24 \times 16$ (Fig. 6.5, Tab. 6.2). The permittivity of this material was measured on plates cutted from C3 (largest) core with sputtered copper electrodes (§ 5.2). In the similar way was obtained the permittivity for the other studied MnZn material 6000HM-1. Measured values of permittivity for both studied ferrite materials are very high (with values of $\varepsilon(0)_{exp} = 1.5 \cdot 10^6$ for 6000HM-1 and $\varepsilon(0)_{exp} = 13.5 \cdot 10^6$ for T37 materials (Tab. 6.2)). Obviously, with these high values of $\varepsilon(0)_{exp}$ the conditions for DR can be realized within sample with moderate dimensions.

The samples were measured so, that windings are covering most of ferrite surface. The dimensional resonance was observed in ferrite cores with relatively large cross section area (C2 and C3 cores), within MHz frequency area (Fig. 6.5), while the C1 core did not showed resonance response.

Table 6.2. Properties of MnZn ferrite cores.

Group	№	Dimensions, mm	A, mm ²	$\varepsilon(0)_{exp}$	$\mu(0)$	$\mu(0)_{exp}$	$D, \mu m$	σ_{mD}
MnZn 6000HM-1	B1	R10 × 4.3 × 10	28.5	1.5×10^6	6000	6750	12.9	0.53
	B2	R20 × 9.1 × 10	54.5	1.5×10^6	6000	6530	12.9	0.53
	B3	R25 × 12 × 10	65	1.5×10^6	6000	6650	12.9	0.53
	B4	R30 × 4.3 × 10	78.5	1.5×10^6	6000	6850	12.9	0.53
	B5	R33 × 10 × 10	115	1.5×10^6	6000	6523	12.9	0.53
MnZn, T37	C1	R12.5 × 7.5 × 5	12.5	13.5×10^6	6500	5800	10.7	0.53
	C2	R20 × 10 × 7	35	13.5×10^6	6500	5900	12.7	0.52
	C3	R40 × 24 × 16	128	13.5×10^6	6000	6000	13.4	0.53

In such a medium, the deciding factor in setting up DR is L : Fig. 6.5 shows that no DR arise (sample C1) if L is small enough but with its growth DR appears and enhances (samples C2, C3) – f_{DR} shifts to lower frequencies and $\dot{\mu}(f) = \dot{\mu}_{ext}(f)$ as extrinsic characteristic gets more and more resonant. It is

particular remarkable that in these processes $\mu(0) \approx const$, that $\dot{\mu}_{ext}(f)$ continues keeping with KKR, that great influence on DR comes from N (Fig. 6.7). It was verified, that influence from N does not come from stray inductance of winding, but is principal (the measured CIP spectra with copper foil windings ($N = 7$) and wire windings ($N = 10$))

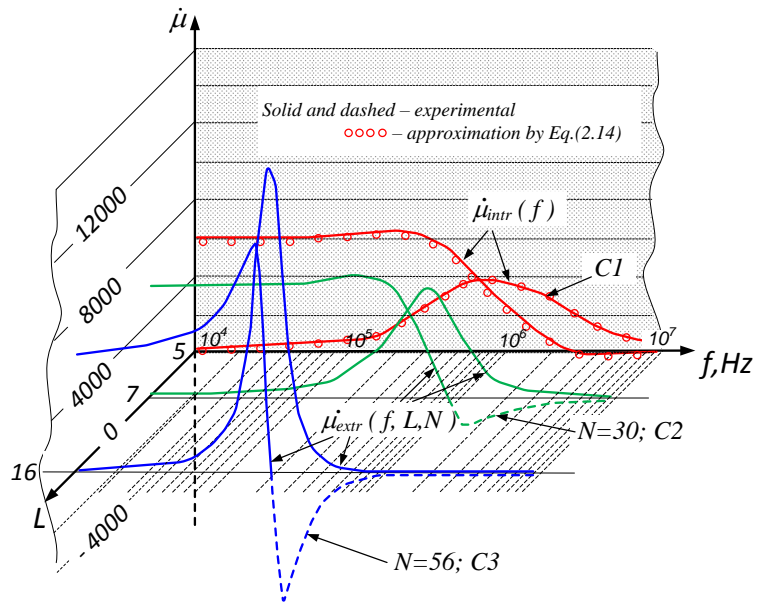


Figure 6.5 The advancement of DR in samples C1...C3 in relation to L and N

showed identical values over whole measured frequency range). Thus, we obtained curves for different winding filled core area, i. e. with different number of winding turns (Fig 6.7). It is seen, that number of winding turns dramatically affects the $\dot{\mu}_{ext}(f, L)$ – for smaller number of turns the DR effect becomes weaker, and the maximal frequency of DR shifts to higher frequencies (Fig. 6.7). This DR dependency from N can be explained based on Eq. 6.1. If inductive PF device is powered by const. voltage, then for higher N the impedance of coil

increases (as N^2), which results in decreased magnetic field and decreased magnetic losses, therefore from Eq. 6.1: λ grows and f_{DR} is shifted to lower frequencies.

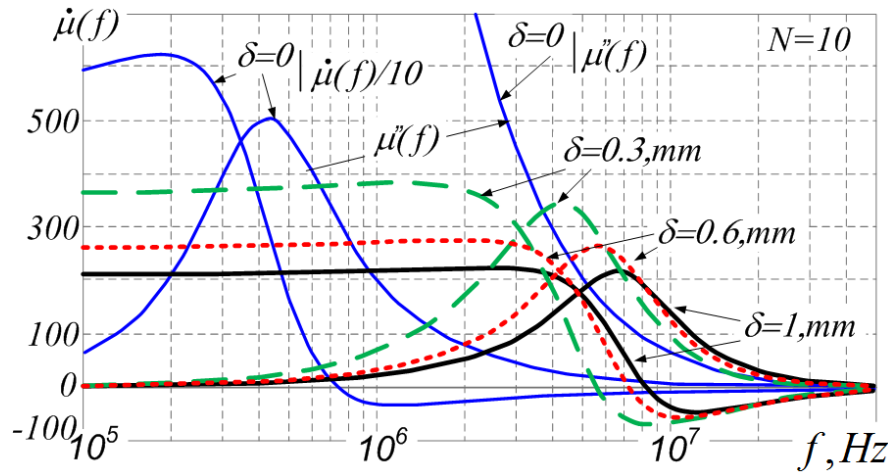


Figure 6.6. Dependence of DR from nonmagnetic gap size δ in C3 core.

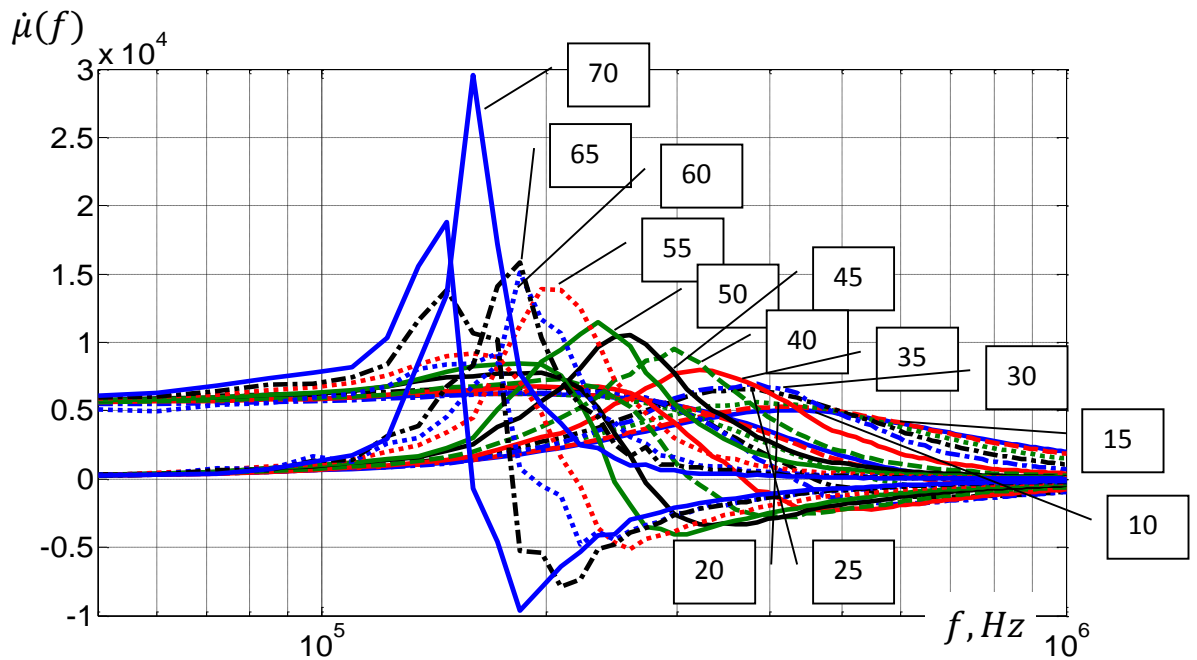


Figure 6.7. Dimensional resonance dependence from turn count N in sample C3.

Introduction of the nonmagnetic air gap in the same (C3) core, as it usually is, shifts CIP spectrum to higher frequencies with Dimensional resonant processes presence in the core (Fig. 6.6). The amplitude is getting smaller and f_{DR} increases with larger gap size. The dependency of DR from N remains valid for all gap sizes.

Yet it can be seen (Fig. 6.6) that the shifting is more pronounced for ascending part of $\mu''_{ext}(f)$ (controlled by coarser grains) than for descending one (ensured by finer grains). This once again (similar as in modelling of $\dot{\mu}_{int}(f)$) shows that coarser grains with their higher

permeability and lower coercivity are more sensitive to excitations, this time to demagnetizing fields.

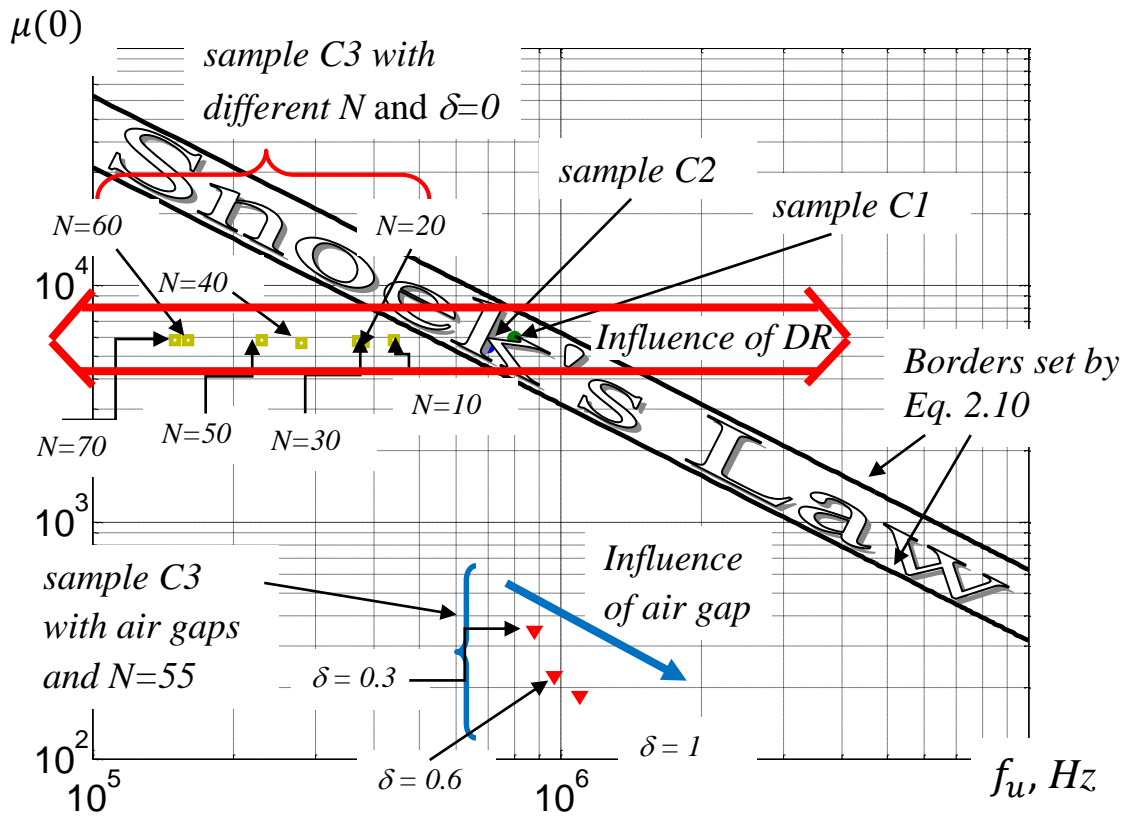


Figure 6.8 Analysis of CIP data of T37 ferrite samples (group C) with of DR on non magnetic gap δ and different winding turn N count for C3 sample.

The collection of CIP data for set of T37 ferrite cores on the one hand matches with standard Snoek's relation (Eq. 2.10;

zone in Fig. 6.8), and does not correlate on the other hand. There C1 sample data is used as reference (as one without the influence of DR and turns number N of winding, representing the material properties; Fig. 6.9) The model parameters of C1 sample are: $\sigma_a = 0.39$ $\sigma_b =$

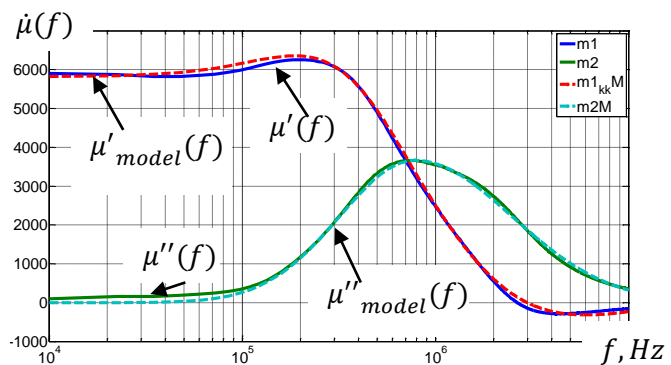


Figure 6.9. Model application to C1 sample.

0.50 , $\sigma_{av} = 0.44$, and this points to good MST quality. The data obtained from micrographs $\sigma_{lnD} = 0.53$ for this sample indeed correlates with the obtained σ_{av} (see Tab. 6.1 and

Tab. 6.2). Yet, evident asymmetric character of CIP spectrum and bigger difference between the σ_{av} and σ_{lnD} shows, that there still are some defects.

In Fig. 6.8 sample C1 appears (as blue dot) in zone of Snoek's Law. For greater dimension samples (e. g., C3) there is seen clear deviation from Snoek's Law type relations on change of N (Fig. 6.8). This once again demonstrates that DR first of all represents the ferrite as the electromagnetic resonator rather than the material substance. In its turn the dependence only on δ seems to follow Snoek's Law type relations (Fig. 6.8, sample C3, $N = const$).

From the above assumptions we can conclude, that DR cannot be removed by applying the nonmagnetic air gap to the core (the gap only shifts the DR to HF together with lowered μ''_{max} (Fig. 6.6)). Thus, by changing the number of winding turns, we can shift the DR, and with lower number of turns DR effect becomes less pronounced (the μ''_{max} changes from 15000 at $N = 70$ to 5000 with $N = 10$).

6.4 Complex initial permeability as intrinsic and extrinsic property

As a whole the application of the model to studied experimental CIP spectra of ferrites as intrinsic property showed good correlation between the model, CIP measurement results and microstructure. The data obtained by the model application to our studied samples is combined in Table 6.1. The outcomes of modelling – successful quantitative estimations of σ_{lnD} from CIP spectrum is of principal importance showing that there really is fundamental connection between the characteristics of CIP and that of MST. The analysis of CIP spectra measured by other scientists revealed that big amount of these spectra belongs to TQG (i. e. [26, 58, 64], a. o.), but still there can be found some samples that are close to IQG (with near-symmetrical CIP spectra and the value of $\sigma \approx 0.5$ [17, 20, 67]).

At the same time the study of CIP as extrinsic properties $\dot{\mu}_{ext}(f)$ reveals that there stands significant distinction from intrinsic properties $\dot{\mu}_{int}(f)$ in response to influential parameters. This results in indirect dependence of $\dot{\mu}_{ext}(f)$ from the intrinsic influence factors, e. g., the microstructure of studied samples. But in opposite to this for extrinsic CIP there is definite influence from the core dimensions and number of measurement winding turns (i. e., the extrinsic factors). The analysis of influence of nonmagnetic air gap to the DR revealed that regardless of the gap size – the DR remains within the core. Thus, the only possible solution found in decreasing the influence of DR to CIP – is to decrease the number of measurement winding turns. Even so – we cannot completely remove this phenomenon (as it is seen from Fig. 6.8 – there still remains difference between C1 sample data and that of C3

with 10 measurement winding turns). Therefore samples B5, C2 and C3 exhibiting dimensional resonance, make CIP to be controlled by extrinsic factors (see Ch. 6.4). This makes it impossible to use the model in present form for the spectra influenced by extrinsic factors.

Thus, the conclusions on the practical use of the model are:

(1) the modelling of $\dot{\mu}_{intr}(f)$ based on effects coming from grain sizes distribution and defects (shorter: MBDD – modelling based on distributions and defects) works well in practice;

(2) the use of the model MBDD gives grounds for the statement that CIP spectra can be applied as qualitative nondestructive method for evaluation of MST: ACp typically have the width (in units of σ): $\sigma_{av} = 0.4 \cdots 0.5$ for high quality laboratory samples, and greater values for industrial ones;

(3) DCp have pronounced negative values ($f > f_u$) for IQG and small or moderate values for TQG (if they are not masked with NSR dispersion);

(4) DW processes indeed are related with the large amplitude dispersion region of CIP spectrum;

(5) in the case of magnetic spectrum with single absorption and dispersion region (when dispersions from DW and NSR processes overlap), parameters σ_a and σ_b of (2.14) are with limited exactness (especially σ_b) and so there is need for further investigations (aimed for more clear separation of DW and NSR contributions).

7 CONCLUSIONS AND FUTURE INVESTIGATIONS

7.1 Conclusions

In the promotion work the applied aspects of analytic presentation of the CIP both for the intrinsic and extrinsic properties of ferrite materials are investigated. A significant part of this work is based on experimental measurements of the complex initial permeability of MnZn and NiZn ferrites (toroidal samples with different dimensions both – factory made-cores and those cut from ferrite tiles). As the result of this work there are proved all of the promoted thesis. Briefly summarizing, the main results of this work can be formulated as follows:

1. All of the experiments were performed in weak excitation fields. So, the measured data correspond to CIP. CIP spectra of the nickel-zinc (NiZn, 4S60) and manganese-zinc (MnZn, 6000HM-1 and T37) ferrites were measured in wide frequency range (from 10^3 – 10^4 to 10^7 – 10^8 Hz), thus covering the large amplitude absorption region of CIP in full measure for correct evaluation of DW component contribution. The obtained results can be used not only for the low-power elements of SMPS (such as common-mode chokes ferrite beads a. o.), but for magnetic components for high frequencies as well.

2. For the CIP measurement both the classical and less labor-saving approaches were used. The CIP spectra obtained with the VNA was compared with the classical measurement methods, such as phase meter and Q-meter measurements, and showed a good correlation between them. All of the obtained CIP spectra was verified by the correspondence to the Kramers-Kronig relations. The correlation turned out to be quite good for all of the studied samples CIP spectra, which proves that the measurement methods used are valid and with a high degree of accuracy. Thus we can conclude that experimental CIP data is correct and the analysis based on the use of this data is valid.

3. The use of Water-jet technology to cut the samples from ferrite tiles was the most appropriate choice of cutting method. As the SEM element analysis of cut samples does not reveal any contamination nor change (e. g., additives, melting) of microstructure (even on the cutting edge).

4. The microstructure of the ferrite samples was examined and analyzed experimentally. The characteristic feature of their MST is that standard deviation of grain size diameter logarithm (σ_{lnD}) has the value close to 0.5. This approximate equality also holds for many other ferrites of different compositions (also studied by other authors). Thus this value

of $\sigma_{inD} \approx 0.5$ is a characteristic value for ferrites with normal MST and may point to homogeneity of MST.

5. The study of NiZn and MnZn ferrites with similar MST revealed, that:

– the MST of NiZn 4S60 ferrite material is with moderate amount of defects in grains and high porosity level (according to micrographs). And the application of the model to these ferrite CIP spectra although proved that there are defects in microstructure (with $\sigma_{av} > 0.5$). The CIP spectra of NiZn ferrite samples remains the same (regardless of the dimensions of the tested sample) if their MST is similar;

– the MST and model parameters of MnZn ferrites (small dimension samples) showed better microstructure quality (with σ_{av} close to 0.5). In its turn the CIP for relatively small and medium MnZn ferrite cores are similar, but f_u shifts to lower frequencies with incrementally increasing dimensions of the sample. That shift of f_u probably is caused by the weak influence of DR. And, the CIP of the largest of tested samples showed clear resonance attributes, which points to appearance of DR.

6. The Kramers-Kronig relations optimization for large amounts of data was successfully developed within the MATLAB® programming language. This proved, that:

– by using the Kramers-Kronig relations, we can evaluate CIP spectra quality (i. e. evaluate the correspondence of ACp and DCp parts), made more clear the noisy measurement data and together with CIP spectra model allow for the spectra reconstruction, which is essential if the measurement equipment does not support all the desired frequency range (or in case, when there is need in combining of various CIP data from different publications).

– KKR also can be used for CIP spectra decomposition to DW and NSR parts, which allows evaluating the spectral components and their contribution to whole CIP spectra.

7. The experimental investigations of CIP as extrinsic properties $\dot{\mu}_{ext}(f)$ (mainly on MnZn T37 material large toroidal cores) reveals its essential difference from $\dot{\mu}_{int}(f)$, its response to influential parameters. The results include that:

– that dimensional resonance in fact is dependent from wound coil turns and from non magnetic air gap.

– the application of the nonmagnetic gap does not remove the DR, the whole CIP is shifted to higher frequencies with the DR remaining;

– the CIP influenced from DR does not follow Snoek's Law type relations;

– the analytical model is applicable within ferrites with normal microstructure till the appearance of the dimensional resonance, when the CIP dependence on MST fades.

The above findings can be used in:

- calculation of ferrite beads active component for EMI suppression (imaginary part with KKR)
- designing of a new type of common mode noise filters for better electromagnetic compatibility;
- for model-based optimization of calculations of common mode chokes for current SMPS;
- for preventing the damage of magnetic components due to dimensional resonance.

Performed analysis reveals PF CIP physical significance. Besides, the analytical model in coup with KKR makes it possible to quantitatively analyze the spectra (which, judging from publications, cannot do other researchers).

7.2 Future investigations

The complex permeability was studied as CIP, so as the next step, there could be performed experiments within stronger magnetic fields in order to obtain dependencies for high power elements of SMPS within high frequencies. Besides there is used a number of empirical parameters for modeling the CIP spectra. Particularly, as such is static permeability $\mu(0)$, for which there still is not known a clear theory (of real processes that determine its value). Thus, the research in this field would be actual as well.

Contrary to the CIP spectra, that were broadly studied and described in this work, a dimensional resonance phenomena was mainly studied experimentally. On possible future study of the dimensional resonance phenomena may come from the electrodynamics point of view. There could be significant practical application for such investigation in the future (for example for regulated AF resonators).

LIST OF LITERATURE

1. Agilent: Vector analyzer basics, 2004
2. Agilent: Анализаторы цепей: полная характеристика линейных цепей.
3. ASTM Standards, Part 11: Metallography; Nondestructive Testing // Philadelphia, Pa. 19103, 1979, p. 205–237
4. Bertotti G. Hysteresis in magnetism. // Accd. Press, San Diego, CA, 1998.
5. Bishop J. E. L. Enchanted Eddy Current Loss due to Domain Displacement. // J. Magn. Mag. Mat. No. 49, 1985, pp. 241–249.
6. Boerekamp J. G., Visser E. G. grain size dependency of the Steinmetz coefficient of soft ferrite power losses // J. PHYS. IV France.– 1997.– Vol. 7. p.– C1-125–C1-126.
7. Borah S., Bhattacharyya N. S. Broadband measurement of complex permittivity of composite at microwave frequencies using scalar scattering parameters // Progress in electromagnetics research M.– 2010.– Vol. 13.– 53–68 p.
8. Brabers V. A. M. Ferrimagnetic Insulations. // In: Handbook of Magnetism and Advanced Materials. Eds. H. Kronmüller, S. Parkin; vol. 4: Novel Materials, 2007. J. Wiley&Sons, 2079–2097.
9. Brander T., Gefer A., Rall B. Trilogy of magnetics. // 4th Ed., Würth Elektronik, 2009.– 704 p.
10. Brockmeyer A., Experimental Evaluation of the Influence of DC-Premagnetization on the Properties of Power Electronic ferrites. // APEC'96 Conf. Proc., Vol. 1, 1996, 454–460 pp.
11. Cruickshank D. B., Microwave materials for wireless applications, // Artech House, 2011;– 221 p.
12. Drogenik M., Znidarsic A., Makovec D. Use of the retarded solution – reprecipitation process to attain a higher initial permeability of MnZn ferrites // J. Anc. Ceram. Soc., 2003, v. 86, pp. 1601–1604
13. Drogenik U., Kolar J. W., Biela J., Heldwein M. L., Ertal H., Friedli T., Round S. D. PWM converter power density barriers // Power Conversion Conference (PCC'07), Nagoya (Japan), April 2007, pp. 9–29.
14. Dunlop C. J. Modeling Magnetic Core Loss for Sinusoidal Waveforms. // Naval Engineer and Master Thesis. Massachusetts, 2008.
15. Eichhorn T. Estimate Inductor Losses Easily in Power Supply Designs. // J. Power Electronics Technology, 2005, pp. 14–24.
16. Epcos Databook, 2008
17. Epstein D. J., Franckiewicz B. Temperature-Dependent lag in polycrystalline Yttrium-Iron Garnet // J. Appl. Phys, 1959, Suppl. to v. 30, No. 4, 295S–296S
18. Ferroxcube, "3F45 Material specification" – Data, pp. 188–190, 2008
19. Fiorillo F., Beatrice C., Bottaucio O., Mauzin A. Approach to magnetic losses and their frequency dependence in Mn-Zn ferrites // Applied Physics Letters, v. 89, 2006
20. Gieraltowski J., Globus A., Domain wall size and magnetic losses in frequency spectra of ferrites and garnets, // IEEE Trans. Magn., vol. MAG-13, no. 5, pp. 1359, 1977.
21. Globus A. Some physical considerations about the domain wall size theory of magnetization mechanisms // Journal de Physique, 1977, v. 38, No. 4, 1–15.
22. Globus A., Duplex P., Initial susceptibility of ferromagnetic materials and topography of DW // Phys. stat. sol. Vol. 31, no. 2, pp. 765–774, 1969.
23. Globus A., Guyot M., Control of the susceptibility spectrum in polycrystalline ferrite materials and frequency threshold of the losses, // IEEE Trans. Magn. Vol. 6, no 3, pp. 614–617, 1970.

24. Gotoh S., Otake T., Fukuda Y., Togawa J. High Performance MnZn Ferrites for Transformer Core Used in Forward Mode Switching Power Supply. // JFE Techn. Rep. No. 16, 2011.
25. Gottstein G. Physical Foundations of Materials Science // Springer-Verlag Berlin Heidelberg, 2004, pp. 303–307.
26. Guyot M., Merceron T., Cagan V., Messeker A., Mobility and/or damping of the DW, // Phys. stat. sol. (a), vol. 106, no. 2, pp. 595–612, 1988.
27. Islam R., Rahman Md O., Hakim M. A., Saha D. K., Saiduzzaman, Noor S., Al-Mamun M. Effect of Sintering temperature on Structural and Magnetic Properties of $\text{Ni}_{0.55}\text{Zn}_{0.45}\text{Fe}_2\text{O}_4$ Ferrites. // Materials Sciences and Applications, 2012, 3, 326–331
28. Jankovskis J. Complex permeability of ferrites correlated with their microstructure // Advances in Sc. & Techn., 2006, v. 45, 2560–2565.
29. Jankovskis J. Empirical Relations. Analogous to Snoek's Law, for Account of Polycrystalline Ferrites Grain Size Effects. // RTU Proc. Series 7., Telecom. and Electr., 2002, pp. 68–76.
30. Jankovskis J. Modelling of Frequency Dependence of Complex Permeability Based on Statistics from Polycrystalline Ferrites Microstructure. // Ferrites: Proc. 8th Int. Conf. (ICF8), pp. 319–321, 2000.
31. Jankovskis J. Presentation of complex permeability spectra of polycrystalline ferrites based on grain size distribution, // J. Magn. Magn. Mat., vol. 272–276, pp. e1847–1849, 2006.
32. Jankovskis J. Relations analogous to Snoek's one, for domain wall processes, // J. Magn. Magn. Mat., vol. 304, pp. e492–e494, 2006.
33. Jankovskis J., Ponomarenko N. Complex permeability of ferrites as intrinsic and extrinsic properties. // J. Chem. Chem. Eng. Vol. 8, 2014, p. 85–91.
34. Jankovskis J., Ponomarenko N., Mironova-Ulmane N., Jakovlevs D. Dimensional effects of sample geometry and microstructure of MnZn and NiZn ferrites. // 2012 IOP Conf. Ser.: Mater. Sci. Eng. 38 012018.
35. Jankovskis J., Ponomarenko N., Mironova-Ulmane N., Jakovlevs D. The study of correlation between microstructure of ferrites and their complex permeability spectra. // 2013 IOP Conf. Ser.: Mater. Sci. Eng. 49 012045.
36. Jankovskis J., Ponomarenko N., Narica P. An Investigation on High Frequency Permeability of Polycrystalline Ferrites. // Proceedings of the 8th International Scientific and Practical Conference, Latvia, 20.–22. June, 2011.– pp 194–201.
37. Jankovskis J., Ponomarenko N., Stepins D. Frequency Dependence of Complex Permeability of Polycrystalline Ferrites Based on the Realities of Microstructure. // 2013, Key Engineering Materials, 543, 507.
38. Jankovskis J., Stepins D., Ponomarenko N. Effects of Spread Spectrum on Output Filter of Buck Converter. // Electronics and Electrical Engineering, 2013, Vol. 19, No. 5, pp. 45–48. e-ISSN 2029-5731. ISSN 1392-1215.
39. Jet Edge waterjet systems. How a Water Jet Machine Works, / http://www.jetedge.com/content.cfm?fuseaction=dsp_applications_101
40. Kazimierczuk. High-Frequency Magnetic Components. Wiley, 2009.
41. Keeping S. design Trade-offs in Integrating an inductor into a Power Module. // Journal of Power solutions, 2011.
42. Kurtz S. K., Carpay F. M. A. Microstructure and normal grain growth in metals and ceramics. Pt. 1. // J. Appl. Phys., 1980, v. 51, No. 11, 5725–5744.
43. Laflin M. High frequency implications for switch-mode DC/DC converter design. // Empirion Design Article, 11 pp., 2007.

44. Lebourgeois R. J.-P. G., Lloret B. High Frequency Mn-Zn Power Ferrites // J. Phys. IV, France 1997, pp. C1-105–C1-108
45. Lee D. W., Wang S. X., Tang Y. J., Hong J. I., Berkowitz A. E. Permeability of Fine Magnetic Particles: Measurements, Calibration, and Pitfalls. // IEEE Trans. Magn., Vol. 42, No. 10, 2006.
46. Lomovs. S. Increasing of accuracy for experimental magnetic spectra of high-permeability ferrites // RTU.– 2003. 71 p.
47. Meuche H., Esguerra M. Correlation between losses, complex permeability and electron diffusion in power ferrites // J. PHYS. IV France.– 1997.– Vol. 7.– C1-95–C1-98. p
48. Microchip. Switch mode power supply (SMPS) topologies Part 1 AN1114 [102]
49. Mitchell D. M., Book Review: Introduction to Power Electronics by Daniel W. Hart, Prentice -Hall Inc., 1997. // IEEE Power Electronics Society Newsletter, July 2000.
50. Mochizuki T., Hirohashi T., Tsumura T., Sasaki I. A multiple-output 400 kHz switching power supply using a new ferrite material H63A // IEEE Trans. Mangetics, Vol. MAG-23, No. 5, September 1987
51. Moses A. J. Advanced soft magnetic materials for power applications. // In: Handbook of Magnetic and Advanced Magnetic Materials, Eds. H. Kronmüller, S. Parkin; vol. 4: Novel Materials, 2007. J. Wiley&Sons, 1926–1942.
52. Mossman P., Deakin I. R., High quality, high stability Manganese-Zinc ferrites. // Ferrites: Proc. Int. Conf., 1970, Japan, pp. 199–202.
53. Mpenou X. 20th Soft Magnetic Materials SMM20 Abstract Book.
54. Nowarowski R., King B. Challanges of designing high-frequency, high-input-voltage DC/DC converters. // Texas Instruments, Analog Applications Journal, vol. 20, pp. 28–31, 2Q 2011.
55. ON Semiconductor. Effects of High Switching frequency on buck regulators. // TND338-D
56. Postupolski T. Topological-and-geometrical approach to the determination of spatial features of granular structure // Prace ITR, 1987, z. 107/87, 2–49.
57. Power Perspective Journal. Resonant Converter IC. EPN issue No. 11, 2011, p. 46.
58. Rado G. T. Magnetic spectra of ferrites // Rev. Mod. Phys., 1953, v. 25, No. 1, 81–89.
59. Radonič V., Blaž N., Živanov Lj. Measurement of complex permeability using short coaxial line reflection method //ACTA PHYSICA POLONICA A,– 2010.– Vol. 117 No. 5.– 820.– 824. p.
60. Roess E., Magnetic properties and microstructure of high permeability Mn-Zn ferrites. // Ferrites: Proc. Int. Conf. (Japan), 1970, pp. 203–209
61. Skutt G. R., High-frequency dimensional effects in ferrite-core magnetic devices. // Ph. D. Dissertation. Blacksburg, Virginia, 1996.
62. Skutt G. R., Lee F. C. Characterization of dimensional effects in ferrite-core magnetic devices // IEEE 0-7803-3500-7/96.– 49–54 p.
63. Skutt G. R., Lee F. C., Breslin J. G. Measurement issues in the characterization of ferrite magnetic material // VPEC seminar series.– 1996.– 1–9 p.
64. Slama J., Shiroky P., Shoka M., et. al., Frequency analysis of nickel based magnetic dielectrics // J. Electr. Eng., vol. 60, no 1, pp. 39–42, 2009.
65. Smith J., Wijn H. P. J. "Ferrites" // Philip's Tehn. library, Eindhoven, 1959.– 313 p.
66. Snelling. E. C., Soft Ferrites: properties and applications. Second edition. // Batterworth &Co. Ltd. 1988
67. Standley K., J. Oxide Magnetic Materials // Oxford, At the Clarendon Press, 1962
68. Van der Bosshe A., Valchev V. C., Inductors and Transformers for Power Electronics. // Taylor and Francis, 2005.

69. Varshney D., Verma K., Kumar A. Structural and vibrational properties of $Zn_xMn_{1-x}Fe_2O_4$ ($x=0.0, 0.25, 0.50, 0.75, 1.0$) mixed ferrites. // *Mat. Chem. Phys.* No. 131, 2011, p. 413–419.
70. Visser E. G., Johnson M. T., P. J. van der Zaag. A new interpretation of the permeability of ferrite polycrystals // In: *Ferrites. Proc. 6th Int. Conf. Ferrites, Tokyo, 1992*, 807–811.
71. WARDjet waterjet univercity / <http://www.wardjet.com/waterjet-university.html>
72. Waseem R. A Practical, Accurate and Very General Core Loss Model for Nonsinusoidal Waveforms. // *IEEE Trans. on Power Electronics*, Vol. 22, No. 1, 2007
73. Waseem R. Ferrite Core Loss for Power Magnetic Components Design. // *IEEE Trans. Magn.* Vol. 27, No. 6, 1991
74. WaterJets.org, / http://waterjets.org/index.php?option=com_frontpage&Itemid=1
75. Yamada S., Otsuki E. Analysis of eddy current loss in MnZn ferrites for power supply // *J. Applied Phys.*, 1997, vol. 81, No. 8, pp. 4791–4793.
76. Yoshida S., Kondo K., Kubodera T. Suppression of GHz Noise Emitted From a Four-Layered PWB With Ferrite-Plated Inner Ground Layer // *IEEE Trans. Magn.* Vol. 44, No. 11, 2008
77. Znidarsic A., Drofenik M. Soft Magnetic Ferrite Materials. // *Materiali in Tehnologije*, 37, 2003, pp. 87–90.
78. Ландау Л. Д., Лифшиц Е. М. Теоретическая физика. Том 8: Электродинамика сплошных сред. // Москва, Наука, 1982.
79. Салтыков С. А. Стереометрическая металлография. Москва, Металлургия 1976
80. Юршевич В. В. Температурные измерения в магнитных спектрах Ni-Zn и Mn-Zn ферритов для Индуктивных элементов// РТУ.– 1987. 185с.